1   **Distinct prefrontal top-down circuits differentially modulate sensorimotor behavior**

2   Rafiq Huda[1#*], Grayson O. Sipe[1], Vincent Breton-Provencher[1], K. Guadalupe Cruz[1], Gerald N.
3   Pho[1], Elie Adam[1], Liadan M. Gunter[1], Austin Sullins[1], Ian R. Wickersham[2] & Mriganka Sur[1*]

4   [1]Picower Institute for Learning and Memory
5   Department of Brain and Cognitive Sciences
6   Massachusetts Institute of Technology, Cambridge, MA 02139, USA.

7   [2]McGovern Institute for Brain Research
8   Massachusetts Institute of Technology, Cambridge, MA 02139, USA.

9   [#]Present address:
10   W.M. Keck Center for Collaborative Neuroscience
11   Department of Cell Biology and Neuroscience
12   Rutgers University, Piscataway, NJ 08854, USA.

13   *Correspondence: rafiq.huda@rutgers.edu and msur@mit.edu

Abstract

Sensorimotor behaviors require processing of behaviorally relevant sensory cues and the ability to select appropriate responses from a vast behavioral repertoire. Top-down modulation by the prefrontal cortex (PFC) is thought to be key for both processes but the precise role of specific circuits remains unclear. We examined the sensorimotor function of anatomically distinct outputs from a subdivision of the mouse PFC, the anterior cingulate cortex (ACC). Using a visually guided two-choice behavioral paradigm with multiple cue-response mappings, we dissociated the sensory and motor response components of sensorimotor control. Projection-specific two-photon calcium imaging and optogenetic manipulations show that ACC outputs to the superior colliculus, a key midbrain structure for response selection, principally coordinate specific motor responses. Importantly, ACC outputs exert top-down control by reducing the innate response bias of the superior colliculus. In contrast, ACC outputs to the visual cortex facilitate sensory processing of visual cues. Our results ascribe motor and sensory roles to ACC projections to the superior colliculus and the visual cortex and demonstrate for the first time a circuit motif for PFC function wherein anatomically non-overlapping output pathways coordinate complementary but distinct aspects of visual sensorimotor behavior.

Introduction

The behavioral repertoire of animals is highly enriched by their ability to learn how to respond to sensory cues to achieve goals such as reward[1-10]. Though seemingly simple, goal-oriented sensorimotor behaviors require coordination of multiple processes. Animals receive a deluge of environmental information at any given moment and can express a wide range of motor behaviors. Hence, sensorimotor control requires attentional mechanisms that prioritize processing of relevant sensory cues and select task-appropriate responses. Studies over the past decades have identified the prefrontal cortex (PFC) as a crucial nexus for coordinating sensorimotor behaviors. Specifically, the PFC is thought to generate top-down signals that facilitate task-specific processing[11-18]. However, a fundamental outstanding question is how the anatomical organization of inputs to and outputs from the PFC enables its proposed role in sensorimotor control.

Previous work using electrical stimulation demonstrates that the same PFC area can both enhance the representation of cortical visual signals, a neurophysiological hallmark of visual attention, as well as facilitate motor responses[14,19-21]. However, electrical stimulation is non-selective and hence these studies do not address whether specific PFC cell populations underlie sensory and motor functions. At the same time, other work suggests that the activity of functionally distinct populations of PFC neurons correlates with distinct components of sensorimotor behavior[16,22]. An intriguing possibility is that sensory and motor functions are subserved by distinct PFC subpopulations that target specific downstream structures.

Recent studies have identified a PFC area in mice, the anterior cingulate cortex (ACC), which is functionally and anatomically poised to exert top-down control over visually guided behaviors. The ACC receives inputs from the visual cortex[23] and exhibits visual responses at single-neuron and network levels[24,25]. Studies employing causal manipulations using chemogenetics or optogenetics show that ACC activity is important for optimal performance on visually guided tasks[18,26-28]. The ACC provides top-down outputs to the visual cortex (VC) and motor-related layers of the superior colliculus (SC)[27-31], a crucial midbrain structure for response selection and other functions[9,32-40]. Importantly, these outputs originate from non-overlapping populations of ACC projection neurons[29], raising the possibility that these output pathways differentially modulate sensorimotor behavior. Surprisingly, optogenetic activation of ACC outputs to the VC or SC enhances the gain of stimulus-driven responses in the VC[27,30], suggesting a role for both pathways in sensory processing. While the function of ACC outputs to the VC in

3

61 modulating cortical visual processing is consistent with previous work[14,16], a similar role for ACC

62 outputs to the SC is harder to reconcile. The intermediate and deep layers of the SC are known to

63 modulate specific motor functions and sensorimotor responses[9,32,36,41-44]. Furthermore,

64 pharmacological inactivation of the SC produces a strong deficit in visual attention without

65 perturbing the associated modulation of visual cortical activity[45]. Thus, the precise contribution of

66 ACC projections to the VC and SC in mediating sensory processing and motor responses remains

67 unclear.

68 Elucidating the function of ACC outputs to the VC and SC in sensorimotor control requires

69 probing the underlying visual processing and motor response components. Here, we establish a

70 two-choice behavioral paradigm that allows us to distinguish these processes by testing mice on

71 different cue-response contingencies. Comparing behavioral deficits induced by projection-

72 specific inactivation of ACC output pathways across task contingencies shows that ACC

73 projections to the SC modulate specific motor responses, while projections to the VC contribute

74 to sensory processing. Remarkably, we find that ACC outputs to the SC facilitate motor responses

75 by reducing the innate response bias of the SC. By using two-photon calcium imaging of ACC

76 inputs/outputs, virus-mediated anatomical tracing, and optogenetics, we delineate specific circuit

77 mechanisms mediating this novel effect.

Results

The caudal ACC is anatomically positioned to contribute to visual sensorimotor behavior

80 The ACC is a midline structure that spans a large extent across the caudo-rostral axis[46]. Although

81 recent studies have implicated the mouse ACC in visual behaviors[18,26-28,30], this PFC region is also

82 associated with other diverse behavioral functions[47-49]. We used rabies virus-mediated anatomical

83 tracing and two-photon calcium imaging to determine if the ACC contains a subregion specialized

84 for visual sensorimotor behaviors. We identified sources of visual inputs to the ACC by injecting

85 rabies viruses encoding GFP and tdTomato into caudal and rostral ACC, respectively (Figure 1A).

86 Although both compartments received inputs from medial higher visual cortex, corresponding to

87 functionally-defined anteromedial and posteromedial areas[50], the caudal ACC also received inputs

88 from the primary visual cortex (Figure 1B-C). Moreover, each compartment received prominent

89 inputs from its contralateral hemisphere (Figure 1D). This anatomical organization suggests that:

90 a) the VC provides visual information to the ACC; b) visual information is integrated in ACC

4

91   activity; and c) visual information is exchanged between the two ACC hemispheres via callosal

92   projections. We tested these predictions using two-photon calcium imaging of VC and callosal

93   axons in the caudal ACC. We unilaterally injected GCaMP6s in the VC or the ACC, and placed a

94   chronic cranial window over the caudal ACC to image visually evoked activity of axons (Figure

95   1E). While VC axons responded to stimuli presented in the contralateral visual field (relative to

96   the site of recording), callosal axons responded preferentially to ipsilateral stimuli (Figures 1F, G;

97   Supplementary Figure 1). Importantly, our callosal axon recordings establish that ACC neurons

98   are visually responsive even in naïve mice, and relay visual information to the opposite

99   hemisphere. Hence, VC and callosal inputs provide information about contra- and ipsilateral visual

100   fields to the ACC, respectively.

101   ACC projection neurons are known to provide top-down outputs to the SC[29,30]. We used

102   anatomical tracing to determine if these projection neurons localize to the same subdivision that

103   receives VC inputs. Injection of a rabies virus encoding tdTomato in the SC showed a high density

104   of back-labeled neurons in the ACC (Figure 1H). SC-projecting ACC neurons (ACC-SC) were

105   located predominantly in the caudal subdivision (Figure 1I). This labeling was observed ipsilateral

106   to the site of injection, establishing the unilateral nature of this projection pathway. Together, our

107   anatomical and functional studies show that the caudal ACC integrates visual inputs and provides

108   outputs to the SC, which could allow this PFC area to contribute to visual sensorimotor control.

109   **A sensorimotor behavioral paradigm for studying sensory processing and motor responses**

110   We tested the role of the caudal ACC in visuomotor control by designing a behavioral paradigm

111   for head-fixed mice inspired by previous work[6,10]. This paradigm assesses sensory processing by

112   requiring mice to detect lateralized (i.e., left or right) visual stimuli. Mice report the spatial location

113   of visual cues by rotating a trackball in one of two directions, additionally allowing us to study

114   motor responses. We define visual cues as contralateral (contra) or ipsilateral (ipsi) based on the

115   side of brain hemisphere under study, which is assumed to be the left side for all figures and text

116   (see Table 1 for targeting details and behavioral performance of mice in specific experiments). We

117   began these experiments with the 'inward' cue-response contingency, in which mice move the

118   presented stimulus to the center of the screen. In later experiments, we trained mice on an

119   'outward' contingency, in which mice move cues to the outside of the screen. For the 'inward'

120   task, mice respond to ipsi cues with clockwise actions and to contra cues with counterclockwise

121   actions (Figure 2A). We used a reaction time task design that allowed mice to make a response as

122   soon as they could after stimulus onset. This minimized potential confounds of short-term memory

123   and extensive movement planning associated with delay tasks[51]. Experienced mice performed well

124   on this task (~80% accuracy), with few timeouts (i.e., incomplete trials in which the ball is not

125   moved to response threshold; note that timeout trials are excluded for quantifying accuracy) and

126   responses with short latencies (~400ms) after stimulus onset (Figure 2B).

127   **Activity of ACC-SC neurons during task performance**

128   We used two-photon calcium imaging to determine how ACC activity relates to sensorimotor

129   control during this task. We placed a chronic window over the ACC of Rbp4-Cre x Ai94D mice,

130   which express the genetically encoded calcium sensor GCaMP6s in layer 5 excitatory neurons

131   (Figure 2C). We analyzed responses of single neurons during four combinations of task cues and

132   actions (contra-counterclockwise, contra-clockwise, ipsi-counterclockwise, and ipsi-clockwise).

133   Individual neurons responded to multiple task variables, yet response amplitudes were modulated

134   for specific cues and actions. For example, the neuron shown in Figure 2D selectively responded

135   on contra cue trials but showed a higher response for clockwise vs. counterclockwise actions. The

136   neuron in Figure 2E was active on both contra and ipsi cue trials as long as the animal selected a

137   clockwise response. This pattern of activation also held at the population level; ACC activity was

138   higher on clockwise than counterclockwise trials for both contra and ipsi cues (Figure 2F, G). We

139   compared how ACC neurons respond to contra or ipsi cues without regard to the action selected

140   by the animal. Overall, ACC neurons had higher activity on contra than ipsi cue trials (Figure 2H).

141   We similarly compared responses on clockwise or counterclockwise trials regardless of which

142   visual cue was presented. This showed that ACC neurons respond preferentially to clockwise

143   actions (Figure 2H). These analyses suggest that, as a population, ACC neurons are preferentially

144   activated by contra cues and clockwise actions during the task.

145   We performed pathway-specific imaging to determine whether and how ACC-SC neurons,

146   identified by injecting a synthetic retrograde tracer into the SC (Figure 3A), respond to specific

147   actions. Examination of single neuron and population responses showed higher activation of ACC-

148   SC neurons on clockwise trials (Figure 3B-E). Next, we used a decoding approach to probe

149   whether ACC-SC activity predicted selected actions (Figure 3F, G). Linear SVM classifiers trained

150   with single-trial activity of ACC-SC neurons performed better than chance at predicting actions.

151   Together, these analyses suggest that ACC neurons convey information about clockwise actions

152   to the SC.

The SC facilitates counterclockwise and the ACC-SC pathway clockwise actions

How does the clockwise action information observed in ACC-SC neurons contribute to task performance? We addressed this question by first examining the role of activity in the SC itself. We virally expressed the inhibitory opsin Jaws[52] in the intermediate and deep layers of the left SC and delivered yellow light (593 nm) through an implanted optic fiber on a randomly selected subset of trials (Figure 4A). Illuminating the brain with light in the absence of an opsin did not produce significant changes in behavior, including in correct and incorrect responses on contra or ipsi cues (Supplementary Figure 2). To assess the effect of photoinhibition, we compared how mice responded to contra and ipsi cue trials under 'laser' and 'no laser' conditions (note that timeout trials, in which mice fail to give a complete response, are excluded from performance accuracy analysis and considered separately). Unilateral photoinhibition of the SC biased responses; inhibition increased incorrect responses on contra cue trials but decreased incorrect responses on ipsi cue trials (Figure 4B). In other words, SC inactivation decreased counterclockwise responses (Supplementary Figure 2A) and increased clockwise responses. These results are consistent with a recent neurophysiology study demonstrating that the activity of left SC neurons encodes counterclockwise actions in a similar task[53]. Reducing SC activity also increased the response time on contra cue trials and decreased the timeout rate on ipsi cue trials (Figure 4B). These results suggest that the left SC facilitates counterclockwise actions.

To determine if the left SC facilitates counterclockwise ball movements regardless of specific learned task contingencies, we tested a separate cohort of untrained mice as they spontaneously moved the ball. Inactivation of the left SC reduced counterclockwise and increased clockwise movements, which were like movements during the task (Supplementary Figure 3). The fact that SC inactivation decreases counterclockwise actions during spontaneous movement shows that this structure exerts an innate response bias and facilitates specific movement directions in head-fixed mice. These results, combined with the effects of SC inactivation during the visually guided task (Figure 4B), demonstrate that the left SC facilitates counterclockwise responses; by extension, the right SC facilitates clockwise responses.

How do direct ACC inputs to the SC modulate task performance? We addressed this question by virally expressing Jaws in the ACC and implanting an optic fiber cannula over the left SC to target ACC-SC inputs for inactivation (Figure 4C). ACC-SC inactivation increased incorrect responses on ipsi cue trials and there was a trend for decreased incorrect responses on contra cue

7

184   trials (Figure 4D). That is, inactivation of left ACC-SC inputs increased counterclockwise actions

185   and decreased clockwise actions. Hence, left ACC-SC inputs normally facilitate clockwise

186   responses, consistent with the physiological responses of ACC-SC neuronal populations (Figure

187   3E-G). Given that the left SC promotes counterclockwise responses (Figure 4B; Supplementary

188   Figure 3) and that each hemisphere of the ACC targets the SC on the same side (Figure 1H), these

189   results suggest that the ACC-SC pathway promotes clockwise actions by reducing

190   counterclockwise responses.

191   The SC facilitates counterclockwise responses (Figure 4B, Supplementary Figure 3); yet,

192   unexpectedly, ACC inputs to the SC facilitate the opposite response (i.e., clockwise actions; Figure

193   4D). Since cortical projection neurons are predominantly glutamatergic, it is unclear how

194   excitatory ACC-SC inputs implement a response bias opposite to the SC itself. We tested how the

195   ACC influences activity in the SC; we photostimulated ChR2-expressing excitatory ACC neurons

196   and used a 16-channel silicone probe to measure responses of SC neurons in the intermediate and

197   deep layers of awake mice (Supplementary Figure 4A). Photostimulation modulated the activity

198   of 27% of SC units (17/63 units from 3 mice) and led to a heterogeneous effect; while some SC

199   units were excited, others were inhibited (Supplementary Figure 4B,C).

200   These optogenetic manipulations could exert their effect indirectly by recruiting

201   polysynaptic inhibitory pathways through the basal ganglia[54], excitatory-inhibitory commissural

202   SC circuitry[55], or other mechanisms. Alternatively, these results may reflect direct effects on SC

203   neurons. We used anterograde trans-synaptic viral tracing[56] to label SC neurons targeted by the

204   ACC. We injected tdTomato reporter mice with an AAV1 virus expressing the Flpo recombinase

205   in the ACC and performed immunohistochemistry against NeuN and GABA in slices containing

206   the SC (Supplementary Figure 4D,E). Overall, $6.6 \pm 1.3\%$ of SC neurons expressed tdTomato (n

207   = 5 mice). tdTomato labeling was observed in both GABA- and non GABA-containing neurons,

208   suggesting that ACC inputs target both excitatory and inhibitory SC neurons. Yet, we found an

209   overrepresentation of GABAergic neurons in our sample of tdTomato positive neurons, as

210   compared to tdTomato negative neurons (Supplementary Figure 4F). Therefore, ACC neurons may

211   recruit both excitatory and inhibitory neurons to modulate SC activity (Supplementary Figure 4G),

212   potentially in a task-dependent manner.

213   **ACC outputs to the visual cortex facilitate performance on contra cue trials**

214   Our results suggest that the ACC-SC pathway facilitates specific responses during the task.

215   Sensory processing of behaviorally relevant stimuli is another key component of visual

216   sensorimotor control. The ACC densely projects to the VC, modulates its activity, and facilitates

217   performance on visually guided sensorimotor tasks[17,18,28,29]. Hence, we determined the function of

218   the ACC-VC pathway in this task. First, we performed retrograde tracing to determine the

219   organization of ACC outputs to the VC and the SC. Injection of red and green fluorophore

220   expressing rabies viruses in the SC and VC, respectively, showed that non-overlapping

221   populations of ACC projection neurons target either structure, suggesting functional

222   differentiation in ACC outputs (Figure 5A). To determine the contribution of the ACC-VC

223   pathway, we first assessed the function of the VC in this task. Unilaterally inactivating the VC by

224   delivering yellow light onto Jaws-expressing neurons increased incorrect responses on contra cue

225   trials (Supplementary Figure 5). While this manipulation did not change the response time, there

226   was an increase in the timeout rate on contra cue trials, consistent with a role for the VC in

227   detection of contralateral visual cues[57]. These results suggest that the ACC may facilitate contra

228   cue performance by modulating activity in VC. We directly tested this hypothesis by expressing

229   Jaws in the ACC and photostimulating ACC output axons in the VC during the task (Figure 5B).

230   Inactivating the ACC-VC pathway increased incorrect responses on contra cue trials (Figure 5C).

231   Directly comparing the effect of inactivating the ACC-SC and ACC-VC pathways showed that

232   ACC outputs to SC increased and outputs to VC decreased counterclockwise responses associated

233   with the contra cue (Figure 5D). Thus, ACC-SC and ACC-VC pathways oppositely control

234   behavioral performance in this task and may differentially modulate sensorimotor behavior.

235   **ACC-SC and ACC-VC pathways differentially modulate sensory processing and motor**

236   **responses**

237   How do ACC-SC and ACC-VC pathways control task performance? Optogenetic inactivation of

238   these pathways can directly modulate specific responses or disrupt processing of visual stimuli

239   that cue responses. We dissociated these possibilities by training a new cohort of mice on a

240   reversed sensorimotor contingency, such that mice were required to move the presented visual cue

241   outward to the side of the screen instead of the center (Figure 6A). In this task, clockwise responses

242   previously associated with an ipsi stimulus were cued by the contra stimulus (and vice versa).

243   Inactivation of the ACC-SC pathway caused a reversal in deficit and increased incorrect responses

244   on contra cue trials (Figure 6B), as opposed to the deficit observed on ipsi cue trials in the previous

9

245   task contingency (Figure 4D). Thus, the ACC-SC pathway facilitates clockwise responses in either

246   task contingency. In contrast, inactivating the ACC-VC pathway increased incorrect responses on

247   contra cue trials (Figure 6C), similar to that observed in the previous task (Figure 5C). Hence, the

248   ACC-VC pathway is important for sensory processing of contra stimuli in both tasks. We did not

249   observe significant changes in timeouts or the reaction time with either manipulation in the

250   outward task (Figure 6B, C).

251   We further determined how deficits observed with ACC-SC and ACC-VC pathways map

252   onto responses to specific visual cues or the direction of the response itself. We combined data

253   across the two tasks and computed a contra stimulus response index to compare how inactivation

254   of ACC-SC and ACC-VC pathways affects responses associated with the contralateral visual cue.

255   Inactivation of the ACC-VC pathway significantly decreased responses cued by contra stimuli,

256   whereas inactivation of the ACC-SC pathway had no consistent effect (Figure 6D). Next, we

257   computed a counterclockwise response index to determine how optogenetic inactivation modulates

258   counterclockwise responses regardless of which stimulus cues them. While ACC-SC inactivation

259   increased counterclockwise responses, we did not observe a significant change with ACC-VC

260   inactivation (Figure 6E). Thus, the ACC-SC pathway mediates specific motor responses, whereas

261   the ACC-VC pathway facilitates sensory processing in these tasks (Figure 6F).

Discussion

262

263   We demonstrate that the ACC modulates visual sensorimotor behaviors by using anatomically

264   distinct but functionally complementary populations of projection neurons to facilitate sensory

265   processing (ACC-VC) and specific motor responses (ACC-SC; Figure 6D-F). We show that VC

266   inputs bring contralateral stimulus information and callosal inputs bring ipsilateral stimulus

267   information to the caudal ACC (Figure 1A-G; Supplementary Figure 1). In turn, a subset of ACC

268   neurons projects to the SC (Figure 1H). Using a two-choice visual sensorimotor task, we show that

269   the activity of ACC-SC neurons predicts actions and responds to clockwise movements (Figure

270   3E,G). SC inactivation decreases counterclockwise responses during the inward task and

271   spontaneous movements (Figure 4A,B; Supplementary Figure 3), consistent with a role for this

272   area in response selection[9,37]. Surprisingly, inactivation of the ACC-SC pathway has the opposite

273   effect and disrupts performance by decreasing clockwise responses (Figure 4D). Importantly, by

274   training mice on a reversed sensorimotor contingency (outward task), we demonstrate that ACC-

10

275 SC inactivation consistently decreases clockwise responses regardless of the specific cue-response

276 mapping (Figure 6B,E). Hence, the ACC-SC pathway primarily contributes to motor responses. In

277 contrast, ACC-VC inactivation decreases performance on contra cue trials in either task (Figure

278 5C, 6C), suggesting that it facilitates contra cue processing regardless of the associated response.

279 The SC is an integrative node within the broader midbrain selection network, serving as a

280 key arbiter for response selection across multiple sensory and motor modalities in many species[9,32-

281 36,42,58]. In our task, mice make responses by rotating a ball with their forepaws. Our finding that

282 SC activity crucially contributes to such responses provides further evidence that the SC plays a

283 general role in the selection of directional responses beyond eye and whole-body movements. We

284 find that unilateral SC inactivation does not increase inaction, but rather changes the likelihood of

285 selecting specific responses (Figure 4B). In other left-right response tasks, neurophysiological

286 recordings show a subset of SC neurons respond maximally for contralateral responses (i.e.,

287 movements directed opposite to the side of hemisphere under study) and are often silent or

288 inhibited for ipsilateral responses[9,53,59]. Similarly, causal activity manipulations produce response

289 biases consistent with these activity measurements[41,42,59]. These results, combined with our own,

290 suggest a 'winner-take-all' interhemispheric competition model for selection in midbrain circuits,

291 wherein the final response is determined by the SC hemisphere with the higher level of activity[9,60].

292 Although the competition process underlying response selection likely involves an interplay

293 between multiple systems, including intrinsic and commissural SC circuitry[58,61,62] and inputs from

294 the basal ganglia[54], our results identify the important role of direct ACC projections to the SC.

295 We found that SC and ACC-SC inactivation oppositely modulates behavioral performance

296 in the inward task contingency (Figure 4B, 4D). Several mechanisms could mediate this effect. In

297 untrained mice, photostimulation of ACC neurons both excites and inhibits a subset of SC units

298 (Supplementary Figure 4A-C). Moreover, ACC outputs directly target inhibitory as well as

299 excitatory SC neurons (Supplementary Figure 4D-F). Hence, one possibility is that ACC

300 projections recruit local inhibition in the left SC on ipsi cue trials (Supplementary Figure 4G),

301 tipping the balance in favor of activity in the right SC and increasing the probability of clockwise

302 responses. Alternatively, this effect may be mediated via commissural excitatory SC neurons[61,62]

303 that are targeted by ACC neurons. In this case, during an ipsi cue trial, activation of left ACC-SC

304 neurons would indirectly increase activity in the right SC (in addition to the ipsi cue directly

305 activating the SC via inputs from the overlying sensory layer and other structures), thereby leading

306   to a clockwise response. A better understanding of the downstream anatomical targets of SC
307   neurons that receive ACC inputs will help clarify these issues. Regardless of exact mechanisms,
308   we clearly demonstrate opposing influence of ACC-SC and SC computations on response
309   selection.

310   A subset of ACC-SC neurons was recently shown to provide collaterals to the lateral
311   posterior (LP) thalamus and modulate cortical sensory processing in the VC[30]. This raises the
312   possibility that ACC-SC neurons are anatomically and functionally heterogeneous. While we
313   clearly demonstrate that direct ACC-SC outputs are critical for facilitating specific motor
314   responses and contribute minimally to sensory processing, it is possible that the sensory function
315   of this pathway was not engaged by the relatively simple visual stimuli used in this task. In contrast
316   to the inward task, we found that the ACC-SC pathway is important for responses on contra cue
317   trials in the outward task contingency (Figure 6B). Hence, task responses of ACC-SC neurons are
318   likely shaped by specific sensorimotor contingencies.

319   Our results also support the hypothesis that the PFC exerts executive control over task
320   responses by modulating activity in downstream motor structures. In the inward task, mice move
321   their forelimbs in a direction that would orient them to the visual cue if they were freely moving,
322   potentially similar to a 'pro' response in eye movement or whole-body orienting tasks[43,63]. In the
323   outward task contingency, mice make movements that orient them away from the visual cue,
324   possibly similar to an 'anti' response. The PFC is thought to play a crucial role in facilitating 'anti'
325   performance[63]. Our projection-specific inactivation of the ACC-SC pathway in the inward and
326   outward task contingencies (Figures 4D; 6B, E) are consistent with a role for the PFC in facilitating
327   'anti' performance.

328   Although ACC outputs to the SC coordinate specific responses, we found that the ACC
329   uses an anatomically non-overlapping but functionally complementary population of projection
330   neurons to facilitate sensory processing through the visual cortex (Figures 5C; 6C,D). An
331   important issue is whether ACC outputs to the VC and SC control behavioral performance by
332   modulating sensory or motor components of the task. Previous studies have addressed this issue
333   using delay tasks with stimulus presentation and motor response epochs separated by an
334   intervening delay[2,5,64,65]. However, in such tasks, the cue-response mapping is known to the subject
335   before stimulus presentation and movement planning can start with stimulus presentation[66],
336   making it difficult to disambiguate whether temporally restricted inactivation affects behavior by

12

337   disrupting sensory or motor processing. We instead addressed this issue by training a set of mice

338   on the outward sensorimotor contingency and comparing the effect of projection-specific

339   inactivation across task conditions. This showed that the ACC-VC pathway is important for

340   responses associated with contralateral visual cues (Figure 6C, D), suggesting it predominantly

341   contributes to sensory processing. This is consistent with previous work demonstrating that the

342   ACC-VC pathway modulates stimulus encoding by VC neurons in passively-viewing mice and

343   facilitates stimulus discrimination[17]. While the exact mechanisms mediating task performance

344   through the visual cortex are unclear, the ACC-VC projection may control VC outputs to multiple

345   pathways that ultimately converge in the SC and other parts of the midbrain selection

346   network[54,67,68].

347   Overall, our results highlight the importance of projection-specific manipulations in

348   multiple task contingencies for dissecting circuit mechanisms underlying sensorimotor behaviors.

349   By dissociating the contribution of individual outputs, our findings suggest a general organizing

350   principle for PFC circuits wherein complementary behavioral functions are fulfilled by

351   anatomically distinct output pathways, thereby enabling independent control over specific

352   functions depending on task demands.

353
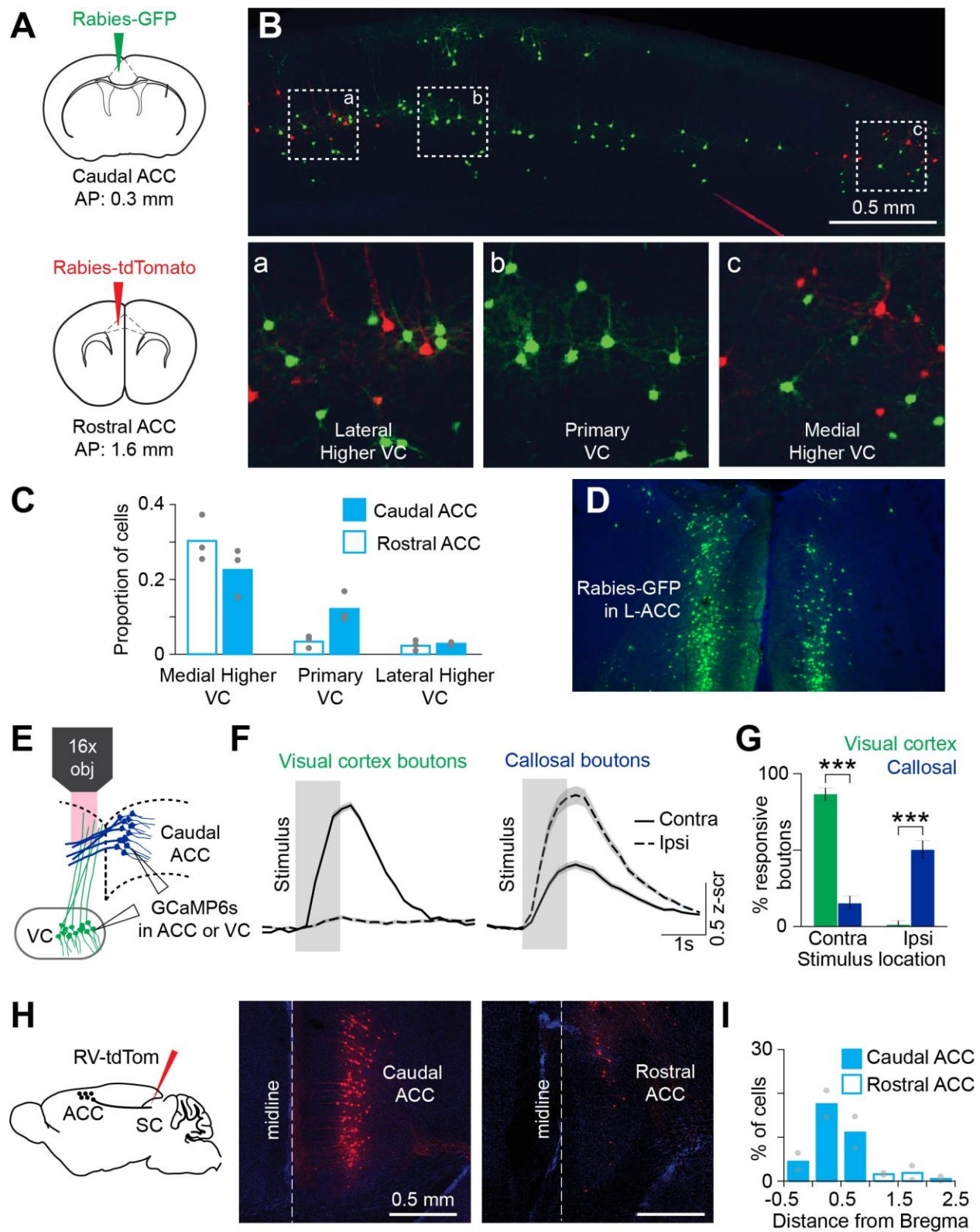
Figure 1. Anatomical and functional characterization of inputs to and outputs from the ACC.

355 (**A**) Rabies viruses encoding GFP or tdTomato were injected into caudal or rostral ACC,
356 respectively.

357 (**B**) Back-labeled neurons in the visual cortex. Neurons in lateral higher VC, primary VC, or medial
358 higher VC are denoted by dotted squares (a-c) on top and shown at higher magnification on the
359 bottom.

360 (**C**) Proportion of back-labeled neurons in various VC subdivisions projecting to caudal (solid) or
361 rostral (unfilled) ACC (n = 3 mice).

362 (**D**) Back-labeled callosal caudal ACC neurons.

363 (**E**) Experimental setup for two-photon imaging of GCaMP6s-expressing visual cortex or callosal
364 axons in the ACC while head-fixed mice passively viewed visual stimuli (black square or grating,
365 ~20°) presented in either hemifield.

366 (**F**) Population-averaged responses of visually-driven VC (n = 268 boutons from 5 mice) and
367 callosal (n = 309 boutons from 4 mice) boutons to stimuli presented in contra- or ipsilateral
368 hemifields. Solid or dashed line is the mean response and shading shows the standard error of the
369 mean.

370 (**G**) Percent of visually-driven VC and callosal boutons with preferential responses to contra or
371 ipsi stimuli. ***$p < 10^{-5}$ (Fisher's exact test, two-sided). Errors bars are 95% binomial confidence
372 intervals.

373 (**H**) Rabies viruses encoding tdTomato were injected in the SC, leading to labeling in the ACC.

374 (**I**) Proportion of back-labeled SC-projecting neurons located along the caudo-rostral axis of the
375 ACC (n = 2 animals).
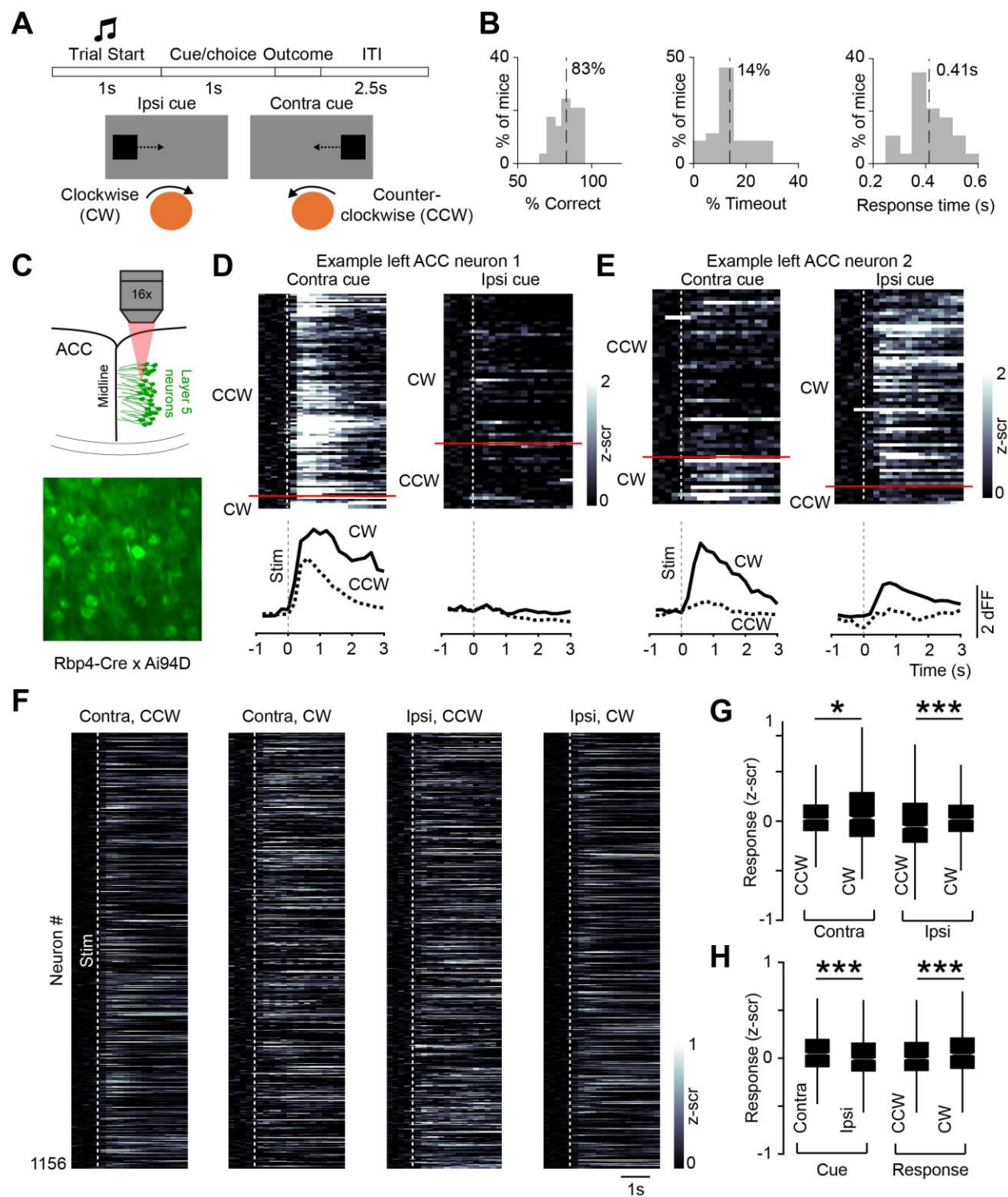
Figure 2. Responses of ACC neurons in a visual sensorimotor task.

(**A**) Trial events during the task (top) and schematic showing the sensorimotor contingency (bottom). Cues are labeled ipsi and contra relative to the brain hemisphere targeted for inactivation/recording (assumed to be the left hemisphere in all figures and the text; see Table 1

381   for targeting details of specific experiments). Mice respond to ipsi and contra cues by rotating a
382   trackball clockwise and counterclockwise, respectively. Counterclockwise action is the correct
383   response for the contra cue but an incorrect response for the ipsi cue (and vice versa for clockwise
384   action). Correct responding moves the cue to the center of the screen, whereas incorrect responding
385   moves it to the side.

386   (**B**) Behavioral performance of mice trained on this task for various optogenetic inactivation
387   experiments (n = 29 mice). Dashed lines indicate mean.

388   (**C**) Two-photon calcium imaging of GCaMP6s-expressing layer 5 neurons. Activity of 1156
389   neurons is reported from 5 expert mice (8 behavioral sessions, 1-3 from each mouse). Dotted lines
390   show stimulus onset.

391   (**D, E**) Activity of two example ACC neurons during the task. Responses on contra and ipsi cue
392   trials with counterclockwise (CCW) or clockwise (CW) actions are shown. Rows correspond to
393   trials.

394   (**F**) Session-averaged activity of individual ACC neurons for the indicated trial type is shown.
395   Each row corresponds to the same neuron across the four plots.

396   (**G**) Average responses on contra and ipsi cue trials with counterclockwise or clockwise responses
397   (contra, CCW vs. CW: p = 0.033, z = -2.1322; ipsi, CCW vs. CW: p = 2.87 x 10^{-7}, z = -5.132). *p
398   < 0.05, ***p < 0.005, Wilcoxon signed-rank test.

399   (**H**) Average responses on contra vs. ipsi cue trials (p = 9.2 x 10^{-9}, z = 5.745) and CCW vs. CW
400   trials (p = 8.3 x 10^{-5} , z = -3.940). ***p < 0.005, Wilcoxon signed-rank test.

17
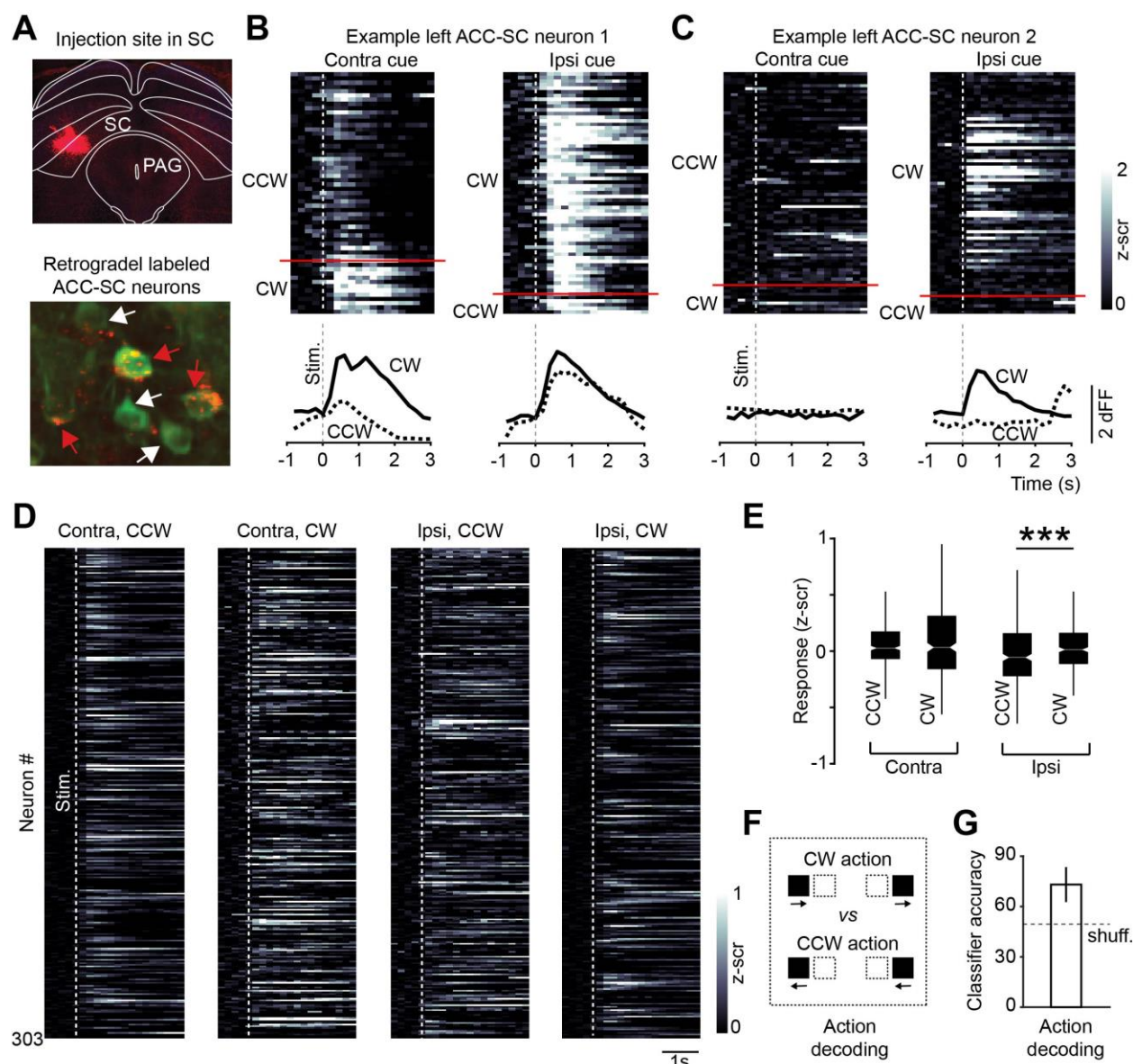
Figure 3. Task activity of ACC-SC neurons.

(**A**) ACC-SC neurons were identified by injecting red retrobeads in SC_m. Recordings were made from 303 ACC-SC neurons in five expert mice (8 behavioral sessions, 1-3 sessions per animal).

(**B, C**) Task responses of two example ACC-SC neurons. Responses on contra and ipsi cue trials with counterclockwise or clockwise actions are shown. Rows show individual trials. Dotted lines show stimulus onset.

(**D**) Session-averaged activity of individual ACC-SC neurons for the indicated trial type. Each row corresponds to the same neuron across the four plots.

410   (**E**) Average responses on contra and ipsi cue trials with counterclockwise or clockwise responses
411   (contra, CCW vs. CW: $p = 0.300$, $z = -1.037$; ipsi, CCW vs. CW: $p = 0.001$, $z = -2.589$). ***$p <$
412   0.005, Wilcoxon signed-rank test.

413   (**F**) Combination of trials used for action decoding. SVM classifier was trained to distinguish
414   responses on clockwise (right arrows) and counterclockwise trials (left arrows). Activity was
415   combined as shown, without regard to the cue condition.

416   (**G**) Classifier accuracy for action decoding. Dotted line shows chance model performance
417   obtained by shuffling trial labels on the test set (see Methods). Error bar shows standard deviation
418   of classifier accuracy over 1000 iterations of the model.
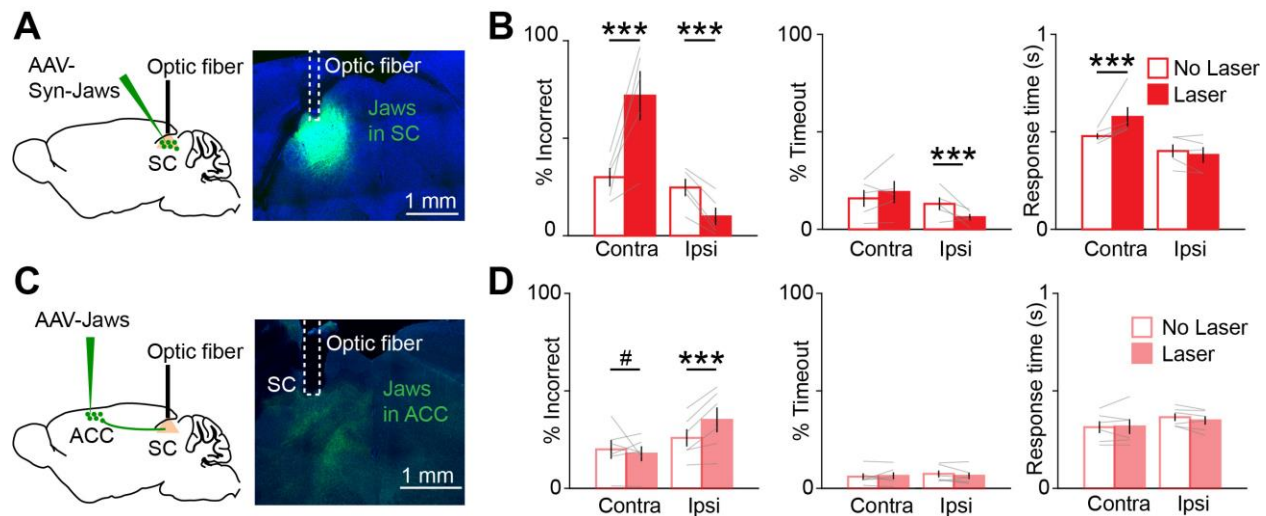
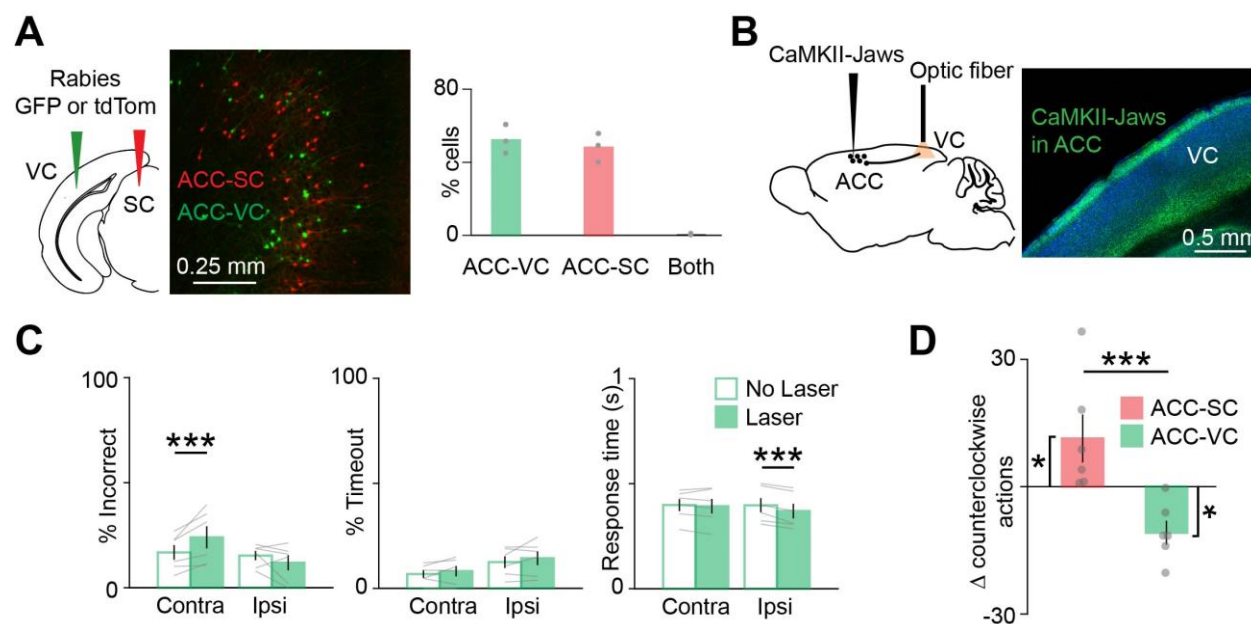**Figure 4. Effect of SC and ACC-SC inactivation on behavioral performance.**

(**A**) AAV5-Syn-Jaws was injected in the SC and a fiber optic was implanted above the injection site.

(**B**) Behavioral performance for non-laser (unfilled) and laser (filled) conditions on contra and ipsi cue trials with SC inactivation (n = 5 mice). Incorrect performance (contra, p = 0.001; ipsi, p = 0.001), timeouts (i.e., trials with incomplete responses within the allotted time; contra, p = 0.077; ipsi, p = 0.001), and response time (contra, p = 0.001; ipsi, p = 0.025) are shown. ***p < 0.005; permutation test.

(**C**) AAV5-CaMKII-Jaws was injected in the ACC and a fiber optic cannula was implanted in the SC.

(**D**) Similar to B, except for inactivation of ACC outputs to SC (n = 6 mice). Incorrect performance (contra, p = 0.061; ipsi, p = 0.001), timeouts (contra, p = 0.961; ipsi, p = 0.561), and response time (contra, p = 0.198; ipsi, p = 0.092) are shown. #p = 0.061, ***p < 0.005; permutation test.

20

Figure 5. Effect of ACC-VC inactivation on behavioral performance.

(**A**) *Left,* Dual-color retrograde tracing from VC and SC. Back-labeled ACC neurons projecting to SC_m (red) or VC (green). *Right,* Proportion of back-labeled neurons projecting to either or both areas (n = 3 mice).

(**B**) AAV5-CaMKII-Jaws was injected in the ACC and axons in VC were targeted for inactivation.

(**C**) Behavioral performance for non-laser (unfilled) and laser (filled) conditions on contra and ipsi cue trials with inactivation of ACC outputs to the VC (n = 6 mice). Incorrect performance (contra, p = 0.002; ipsi, p = 0.153), timeouts (contra, p = 0.204; ipsi, p = 0.312) and response time (contra, p = 0.656; ipsi, p = 0.006) are shown.

(**D**) Comparison of normalized laser-induced change in counterclockwise actions with inactivation of ACC outputs to SC and VC (ACC-SC vs. zero, n = 6 mice, p = 0.046, z = -1.992; ACC-VC vs. zero, n = 6 mice, p = 0.028, z = 2.201; ACC-SC vs. ACC-VC, p = 0.003, z = 2.802). Significance testing with permutation test in C; in D, comparison against zero with two-tailed Wilcoxon signed-rank test and comparison between ACC-SC and ACC-VC with one-tailed Wilcoxon rank-sum test. Error bars are standard error of the mean.
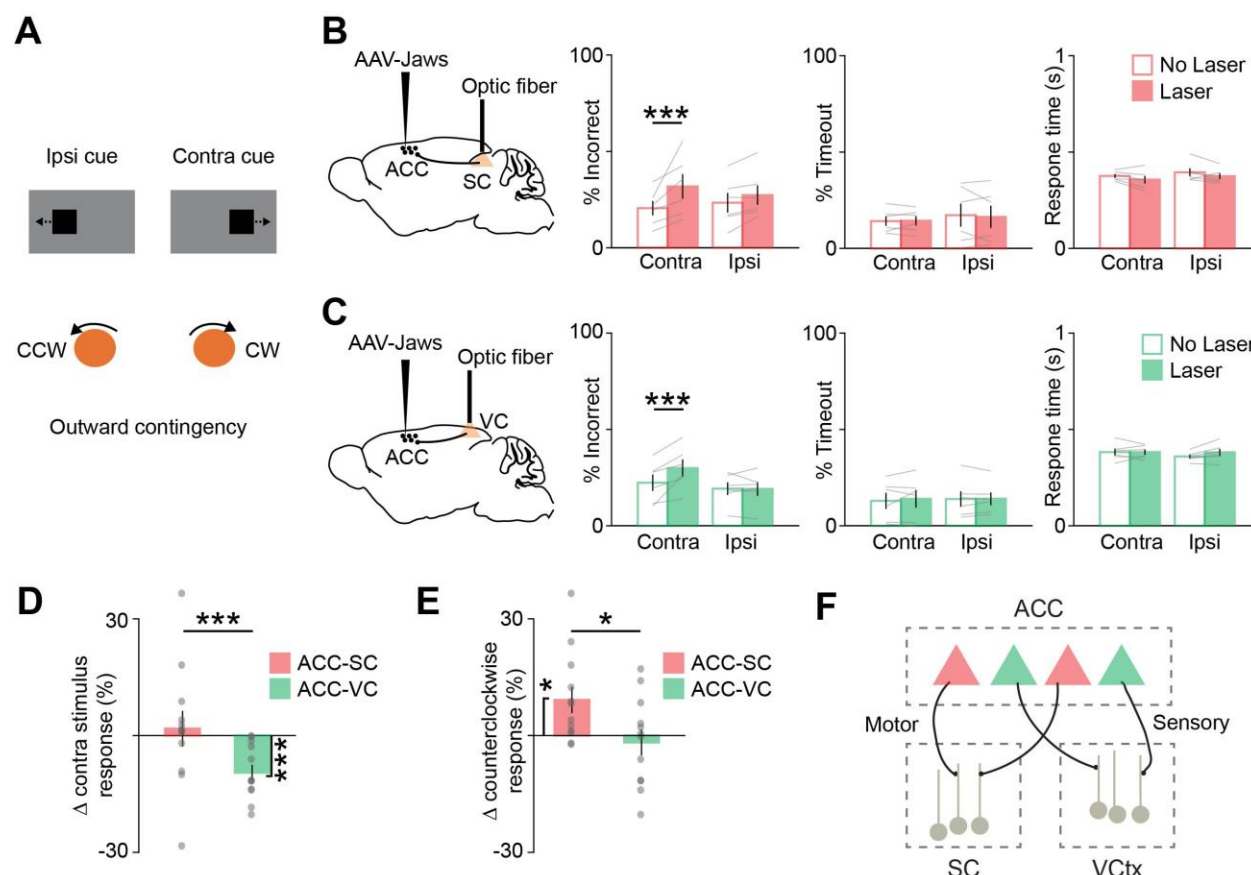
Figure 6. ACC outputs to SC and VC differentially modulate motor and sensory processing, respectively.

(**A**) Mice were trained on the outward sensorimotor contingency and were required to move ipsi and contra cues away from the center by rotating the trackball counterclockwise and clockwise, respectively. Note that in this task, a counterclockwise action is the correct response for ipsi cues but an incorrect response for contra cues.

(**B**) Behavioral performance for non-laser (unfilled) and laser (filled) conditions on contra and ipsi cue trials with inactivation of ACC outputs to the SC in the outward task (n = 6 mice). Incorrect performance (contra, p = 0.001; ipsi, p = 0.127), timeouts (contra, p = 0.924; ipsi, p = 0.927), and response time (contra, p = 0.033; ipsi, p = 0.138) are shown. ***p < 0.005; permutation test.

(**C**) Similar to B, except for inactivation of ACC outputs to the VC (n = 6 mice). Incorrect performance (contra, p = 0.002; ipsi, p = 0.786), timeouts (contra, p = 0.499; ipsi, p = 0.885), and response time (contra, p = 0.869; ipsi, p = 0.042) are shown. ***p < 0.005; permutation test.

(**D**) Data from both tasks was combined. Effect of ACC-SC (n = 12 mice) and ACC-VC inactivation (n = 12 mice) on laser-induced change in contra stimulus responses (ACC-SC vs. zero, p = 0.638, z = -0.471; ACC-VC vs. zero, p = 0.002, z = 3.059; ACC-SC vs. ACC-VC, p = 0.004, z = 2.685). ***p < 0.005; comparison against zero with two-tailed Wilcoxon signed-rank test, and comparison between ACC-SC and ACC-VC with one-tailed Wilcoxon rank-sum test.

22

468   (**E**) Similar to D, except showing laser-induced change in counterclockwise responses (ACC-SC
469   vs. zero, p = 0.019, z = -2.353; ACC-VC vs. zero, p = 0.695, z = 0.392; ACC-SC vs. ACC-VC, p
470   = 0.03, z = 1.876). *p < 0.05; comparison against zero with two-tailed Wilcoxon signed-rank test,
471   and comparison between ACC-SC and ACC-VC with one-tailed Wilcoxon rank-sum test.

472   (**F**) Model summarizing the sensory and motor roles of ACC projections to the VC and SC,
473   respectively.

474
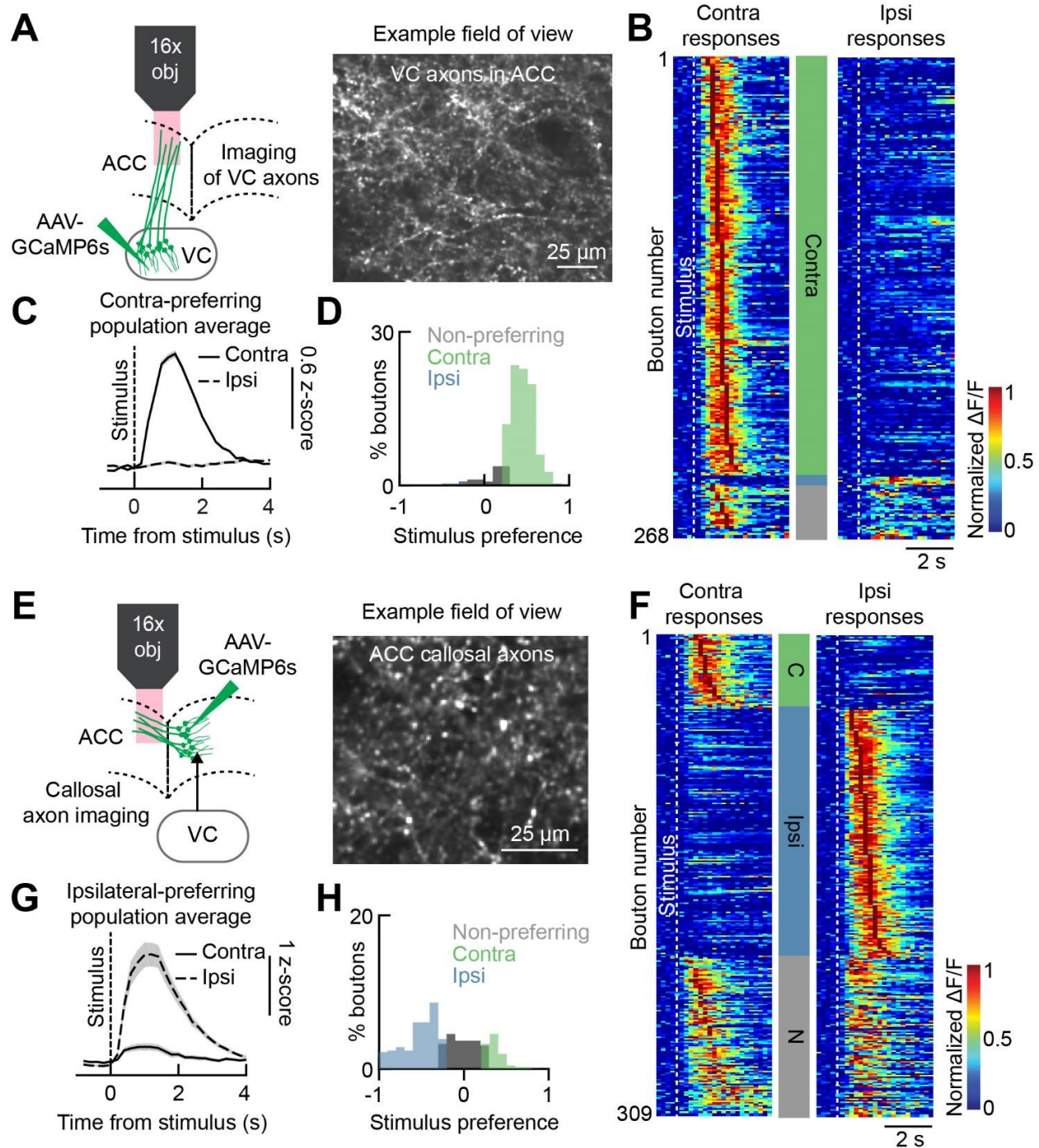
Supplementary Figure 1. Visually-evoked responses of VC and callosal inputs to the ACC.

(**A**) Two- photon calcium imaging of GCaMP6s-expressing VC axons in the ACC.

(**B**) Session-averaged responses of individual visually-responsive boutons to stimuli presented in hemifield contra- or ipsilateral to the recording site (black square, ~20º size, 1s). Responses are grouped by their stimulus preference (contralateral, green; ipsilateral, blue, non-preferring, gray) and sorted within each group by their peak response time.

481   (**C**) Population-averaged response of contra-preferring boutons to contralateral (solid line) and
482   ipsilateral (dashed line) stimuli. Shading shows the standard error of the mean.

483   (**D**) AUROC analysis was used to calculate a stimulus preference score for each visually-
484   responsive bouton. This score ranges from -1 (ipsi selective) to 1 (contra selective). Distribution
485   of scores for 268 visually-responsive VC boutons in ACC from 4 mice is shown.

486   (**E-H**) Same as **A-D**, except for callosal boutons (n = 309 boutons from 5 mice).
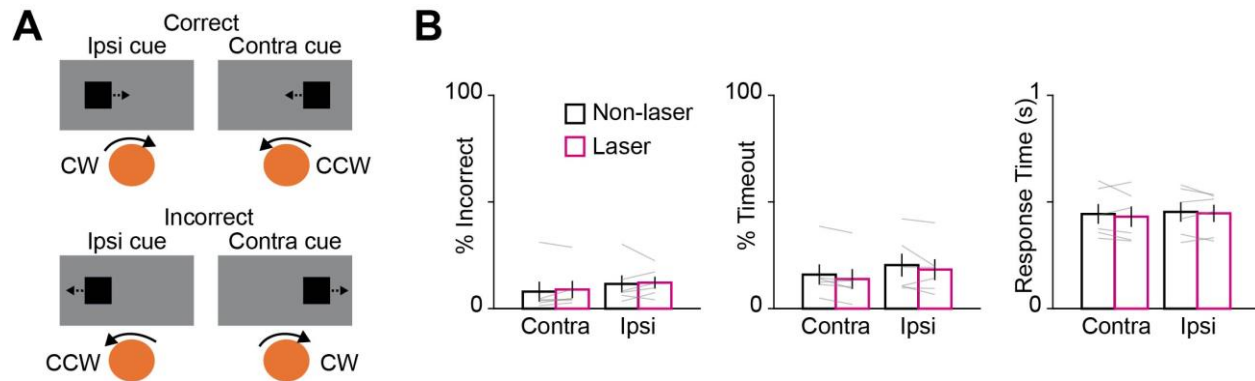
Supplementary Figure 2. Effect of light delivery on behavioral performance.

(**A**) Schematic depicting correct and incorrect responses on the inward task.

(**B**) Behavioral performance with light delivery (20mW) in the absence of opsins (n = 6 mice). Behavioral performance for non-laser and laser conditions on contra cue and ipsi cue trials. Incorrect performance (contra, p = 0.201; ipsi, p = 0.842), timeouts (contra, p = 0.998; ipsi, p = 0.078), and response time (contra, p = 0.527; ipsi, p = 0.647) are shown. Significance testing with permutation test.
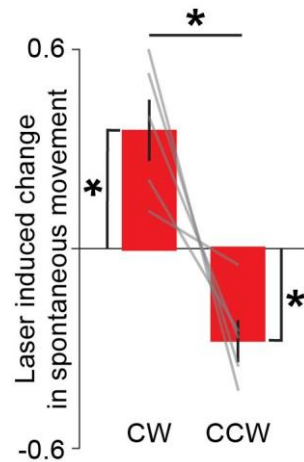
Supplementary Figure 3. SC inactivation during spontaneous movement.

AAV5-Syn-Jaws was injected in the SC and a fiber optic was implanted over the injection site. Laser induced changes in clockwise and counterclockwise actions during spontaneous movements are shown (CW vs. zero: p = 0.018; CCW vs. zero: 0.012; CW vs. CCW: 0.014; n = 5 mice). *p < 0.05; one-sample t-test against zero, and two sample t-test for comparison between actions. Error bars are standard error of the mean.

503
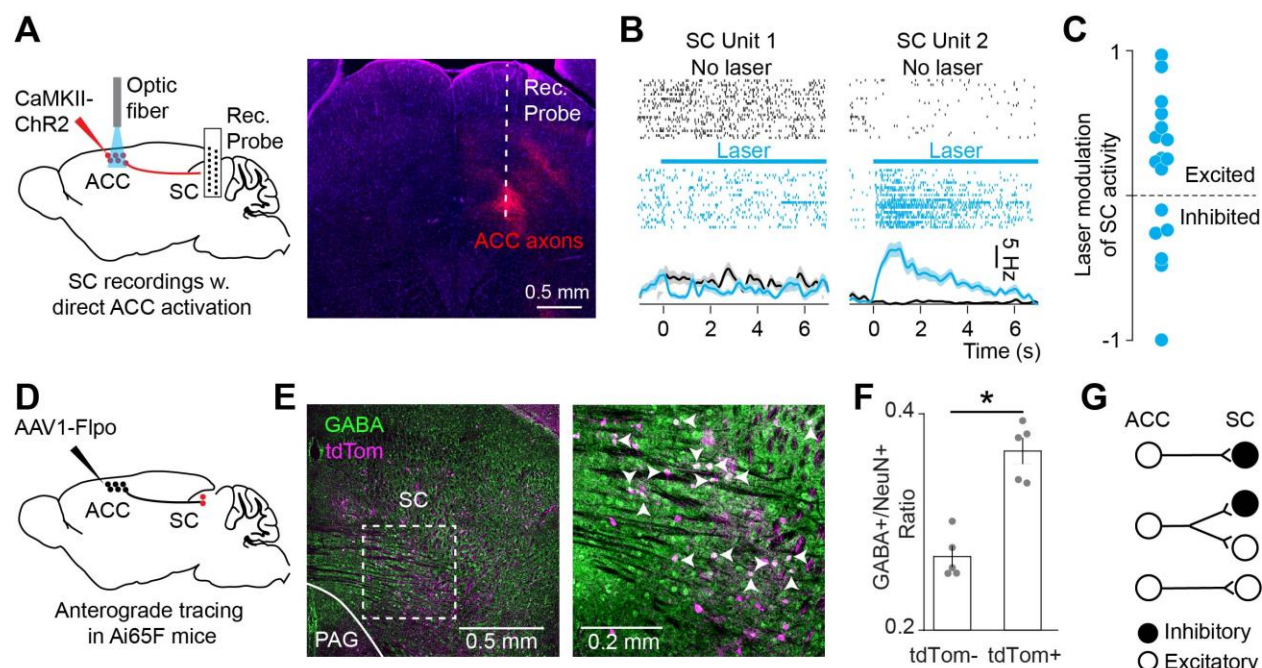
Supplementary Figure 4. Effect of ACC activation on SC activity.

(**A**) AAV virus encoding CaMKII-ChR2-mCherry was injected unilaterally in the ACC and an optic fiber was implanted above the injection site. Extracellular recording probe was inserted in the SC on the same side as the ACC optic fiber.

(**B**) Activity of two example SC units with and without photostimulation of the ACC.

(**C**) Laser-modulation indices for SC units significantly modulated with ACC photoactivation.

(**D**) SC neurons receiving inputs from the ACC were labeled by injecting AAV1-Flpo virus in the ACC of tdTomato reporter mice.

(**E**) *Left,* SC neurons labeled with tdTomato (magenta). Imunnohistochemistry against GABA (green) shows inhibitory neurons. *Right,* higher magnification image of the area bounded by the dotted white square in left panel. Arrowheads mark neurons double-labeled with tdTomato and GABA.

(**F**) Proportion of tdTomato unlabeled (tdTom-) and labeled (tdTom+) neurons (i.e., NeuN positive cells) that are co-labeled with GABA (*p = 0.0431, z = -2.023). Significance testing with two-tailed Wilcoxon signed-rank test. Error bars are standard error of the mean.

(**G**) Proposed circuit schematic for ACC connectivity with excitatory and inhibitory SC neurons.

520
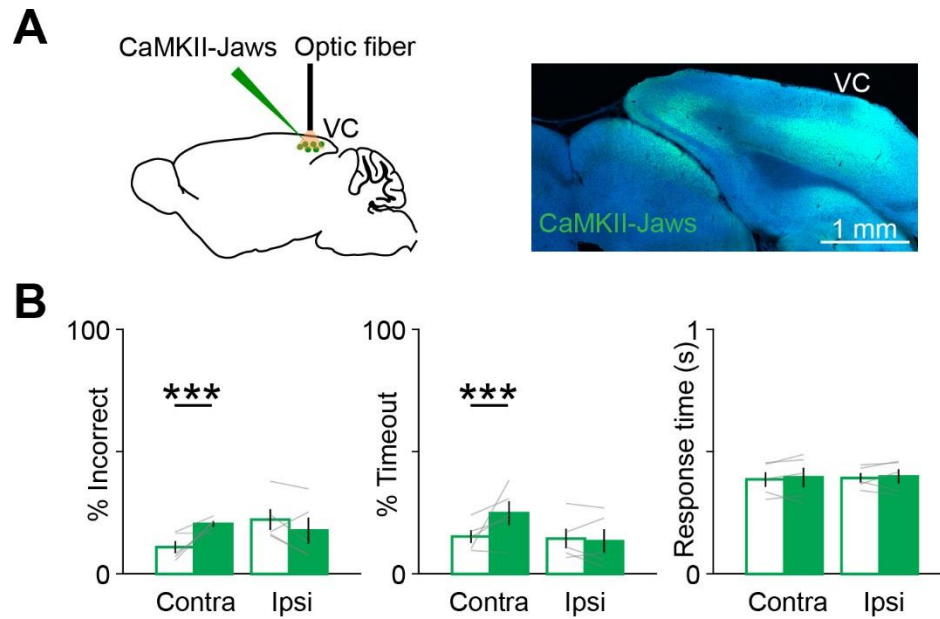
Supplementary Figure 5. Effect of VC inactivation on task performance.

(**A**) AAV5-CaMKII-Jaws was injected in the VC, which was inactivated via yellow light through a chronic window.

(**B**) Behavioral performance for non-laser (unfilled) and laser (filled) conditions on contra and ipsi cue trials with inactivation of the VC (n = 5 mice). Incorrect performance (contra, p = 0.001; ipsi, p = 0.117), timeouts (contra, p = 0.001; ipsi, p = 0.496), and response time (contra, p = 0.232; ipsi, p = 0.966) are shown. Significance testing with permutation test. Significance evaluated at the Bonferroni-adjusted α-value of 0.025. ***p < 0.005.

29

529 **Table 1. Performance metrics of mice included in this study.**

Mouse #	Experiment	Figure[a]	Implant/ imaging site	Behavioral performance			
				Control accuracy[b]	Non-laser accuracy	Timeout	Response Time (s)
61	Light Ctrl	F4-S1	Left	97%	95%	8%	0.35
62	Light Ctrl	F4-S1	Left	87%	93%	16%	0.5
72	Light Ctrl	F4-S1	Left	93%	87%	28%	0.39
100	Light Ctrl	F4-S1	Left	98%	95%	12%	0.32
120*	Light Ctrl	F4-S1	Right	78%	78%	32%	0.53
122	Light Ctrl	F4-S1	Left	93%	94%	10%	0.57
15	SC inh.	F4	Left	65%	61%	4%	0.44
68	SC inh.	F4	Left	76%	76%	12%	0.46
120*	SC inh.	F4	Left	76%	62%	20%	0.48
125	SC inh.	F4	Left	77%	67%	14%	0.36
126	SC inh.	F4	Left	82%	78%	20%	0.41
21*	ACC-SC inh.	F4	Left	85%	69%	6%	0.41
23*	ACC-SC inh.	F4	Left	92%	77%	5%	0.35

30

103	ACC-SC inh.	F4	Left	94%	80%	8%	0.28
104	ACC-SC inh.	F4	Left	98%	93%	14%	0.36
110	ACC-SC inh.	F4	Left	85%	73%	5%	0.26
116*	ACC-SC inh.	F4	Right	75%	65%	3%	0.35
38	Imaging	F2,3	Left	83%	NA	16%	0.49
39	Imaging	F2,3	Left	88%	NA	19%	0.35
41	Imaging	F2,3	Left	84%	NA	24%	0.3
42	Imaging	F2,3	Left	92%	NA	20%	0.37
43	Imaging	F2,3	Left	76%	NA	13%	0.44
8	VC inh.	F5-S1	Left	97%	85%	12%	0.35
9	VC inh.	F5-S1	Left	95%	85%	18%	0.34
20	VC inh.	F5-S1	Left	89%	87%	9%	0.4
19	VC inh.	F5-S1	Left	97%	85%	17%	0.45
33	VC inh.	F5-S1	Left	97%	73%	24%	0.41

21*	ACC-VC inh.	F5	Right	90%	79%	6%	37%
22	ACC-VC inh.	F5	Right	90%	91%	12%	0.48
23*	ACC-VC inh.	F5	Right	92%	89%	6%	0.36
107	ACC-VC inh.	F5	Left	96%	90%	14%	0.29
114	ACC-VC inh.	F5	Right	75%	75%	15%	0.47
116*	ACC-VC inh.	F5	Right	75%	76%	8%	0.38
117*	ACC-SC Rev.	F6	Left	81%	71%	6%	0.35
118*	ACC-SC Rev.	F6	Left	88%	89%	28%	0.37
119*	ACC-SC Rev.	F6	Left	71%	69%	12%	0.42
127*	ACC-SC Rev.	F6	Right	79%	74%	11%	0.38
129*	ACC-SC Rev.	F6	Right	76%	68%	18%	0.38
153*	ACC-SC Rev.	F6	Right	86%	84%	18%	0.38
117*	ACC-VC Rev.	F6	Right	81%	80%	22%	0.38
118*	ACC-VC Rev.	F6	Right	88%	91%	16%	0.38
119*	ACC-VC Rev.	F6	Right	71%	72%	6%	0.36
127*	ACC-VC Rev.	F6	Left	79%	72%	4%	0.36

| 129* | ACC-VC Rev. | F6 | Left | 76% | 71% | 16% | 0.41 |
| 153* | ACC-VC Rev. | F6 | Left | 86% | 83% | 18% | 0.35 |

530

531   * Mice contributed data to two experiments

532   [a] First figure referencing data from each mouse

533   [b] Accuracy on control trials from non-optogenetic sessions

Acknowledgments

543 **Author contributions**

544 R.H. and M.S. conceived the project and developed the concepts presented. R.H. designed the

545 experiments and analysis approach with contribution from M.S. R.H. and G.P. designed and

546 implemented the behavioral task. R.H. performed and analyzed the anatomical, behavioral,

547 optogenetic, and calcium imaging experiments with contributions from G.O.S., K.G.C., L.G., A.S.,

548 and E.A. V.B.P. performed and analyzed the extracellular recording experiments with input from

549 R.H. I.C.W. provided unpublished reagents. R.H. and M.S. wrote the manuscript with input from

550 all authors.

551 **Declaration of interests**

552 The authors declare no competing interests.

Methods

Animals: All experimental procedures performed on mice were approved by the Massachusetts Institute of Technology Animal Care and Use Committee. Mice were housed on a 12 hour light/dark cycle. Animals were group-housed before surgery and singly-housed afterwards. Adult mice (> 2 months) of either sex were used for these studies. In addition to wild type mice, the following transgenic lines were used: Rbp4-Cre (MMMRC stock # 031125), Ai94(TITL-GCaMP6s)-D (Jackson Laboratory stock # 024104), and Ai65(RCFL-tdT)-D (Jackson Laboratory stock # 021875).

Surgical procedures: Surgeries were performed under isoflurane anesthesia (3-4% induction, 1-2.5% maintenance). Animals were given analgesia (slow release buprenex, 0.1mg/kg and Meloxicam 0.1mg/kg) before surgery and their recovery was monitored daily for 72 hours. Once anesthetized, animals were fixed in a stereotaxic frame. The scalp was sterilized with betadine and ethanol. For anatomical tracing experiments, we made a midline incision in the scalp using a scalpel blade. Depending on the experiment, rabies or AAV viruses were injected in the visual cortex (AP: -3.5mm, ML: 2.5mm, DV: 0.5 mm), caudal ACC (AP: 0.3mm, ML: 0.5mm, DV: 0.5 mm), rostral ACC (AP: 1.6mm, ML: 0.3mm, DV: 1.3 mm), or the superior colliculus (at AP: -3.6mm, ML: 1mm, and DV: 1.5mm) using a microinjector (Stoelting). After virus injection, the scalp was reclosed with sutures and skin adhesive (Vetbond).

The following surgical procedures were performed for optogenetics or imaging experiments. For experiments requiring the use of dental acrylic (fiber optic cannulae and chronic imaging windows), we removed a portion of the scalp using spring scissors, scraped away the periosteum membrane overlying the skull, and used a dental drill to abrade the skull to improve adhesion. For light control experiments, two mice expressed axonal GCaMP6s and four mice were wildtype (Supplementary Figure 2B). For photoinhibition of the superior colliculus (SC) during the inward task or spontaneous movements, we injected AAV5-hSyn.Jaws-KGC-GFP-ER2 (100nL) in the intermediate/motor layer (AP: -3.6mm, ML: 1mm, DV: 1.5mm) and implanted a fiber optic cannula (300µm/0.39NA core, CFM13L02, Thorlab) 0.2mm dorsal to the injection site. Cannulae were secured on the skull using layers of Metabond and were protected with a dust cap until used for experiments. For modulating ACC outputs to the superior colliculus, we injected AAV5-CaMKII-Jaws-KGC-GFP-ER2 (University of North Carolina vector core) in the ACC and implanted a fiber optic cannula (300µm/0.39NA core or 400µm/0.5 NA core, CFMXD02,

35

584 Thorlabs) over the intermediate layer of the superior colliculus (AP: -3.6mm, ML: 1mm, DV:

585 1.3mm). For optogenetic inactivation of the visual cortex (VC), we drilled a 3mm craniotomy and

586 made 8-12 injections (100nL each) of an AAV5.CaMKII.Jaws-KGC-GFP-ER2 (University of

587 North Carolina vector core) virus 0.5mm below the surface in a grid pattern. Injections were

588 centered on the left primary visual cortex (centered at AP: -3.5mm, ML: 2.5mm; range AP: 4 to

589 3mm, ML: 2.2 to 2.8mm). For inactivation of ACC axons in VC, we injected AAV5-CaMKII-

590 Jaws-KGC-GFP-ER2 in the ACC and implanted a 3mm chronic window or a fiber optic cannula

591 (400μm/0.5 NA core) over the VC (centered at AP: -3.5mm, ML: 2.5mm, AP = 0, on pia). In a

592 subset of experiments on the inward task, AAV5-CaMKII-Jaws-KGC-GFP-ER2 was injected

593 bilaterally in the ACC and the VC or SC was targeted for axonal inactivation on either side of the

594 brain. For projection-specific optogenetic inactivations during the outward contingency task, we

595 bilaterally injected AAV5-CaMKII-Jaws-KGC-GFP-ER2 in the ACC and implanted fiber optic

596 cannulas over the SC and VC on either side of the brain (see Table 1 for details on which brain

597 hemisphere was targeted for each experiment).

598 For all imaging experiments in the ACC, we drilled a 3mm craniotomy over the midline

599 (centered at AP: 0.5mm and ML: 0mm) and implanted a chronic imaging window assembled from

600 two 3mm coverslips glued to a 5mm coverslip using a UV curable adhesive (Norland 61; double-

601 chronic window). Two 3mm coverslips were required to minimize movement artifacts for GCaMP

602 recordings during task performance. To label superior colliculus-projecting ACC neurons (ACC-

603 SC), we injected 100nL of red retrobeads (Lumaflour) in the intermediate/motor layer of the SC

604 (at AP: -3.6mm, ML: 1mm, DV: 1.7mm). For axonal imaging experiments, 200nL of AAV1-Syn-

605 GCaMP6-WPRE-SV40 virus was injected unilaterally in the visual cortex (AP: -3.5mm, ML: 2.5

606 mm, DV: 0.5 mm) or the opposite ACC (AP: 0.5mm, ML: 0.5 mm, DV: 0.5 mm).

607 For all experiments, after implantation of chronic windows or optic fiber cannulas, the skull

608 was attached to a stainless-steel custom-designed head plate (eMachines.com) using Metabond.

609 Animals were allowed to recover for at least five days before commencing water restriction for

610 behavioral experiments.

611 Virus-mediated anatomical tracing: Standard histological techniques were used for analysis of

612 retrograde and anterograde transsynaptic tracing experiments and for post-hoc verification of

613 implantation/injection sites. Mice were deeply anesthetized with isofluorane and transcardially

614 perfused with a 4% paraformaldehyde (PFA) solution prepared in phosphate buffered saline (PBS).

615   Extracted brains were postfixed in 4% PFA overnight at 4°C, then kept in PBS until sectioning.

616   Fixed brain tissue was sectioned using a microtome (Leica VT-1000) into coronal slices (thickness

617   of 50-100 µm, depending on the experiment). Slices were stained with DAPI and mounted on glass

618   microslides using Vectashield hardset mounting media. Mounted sections were stored at 4°C until

619   they were imaged using a laser scanning confocal microscope (Leica SP8).

620   Rabies viral vectors were made as described[69]. Briefly, HEK 293T cells (ATCC CRL-

621   11268) were transfected with expression vectors for the ribozyme-flanked viral genome (cSPBN-

622   4GFP (Addgene 52487) or pRVΔG-4tdTomato (Addgene 52500)), rabies viral genes (pCAG-

623   B19N (Addgene 59924), pCAG-B19P (Addgene 59925), pCAG-B19G (Addgene 59921), and

624   pCAG-B19L (Addgene 59922)), and the T7 polymerase (pCAG-T7Pol (Addgene 59926)).

625   Supernatants were collected from 4 to 7 days after transfection, filtered, and pooled, passaged 3-4

626   times on BHK-B19G2 cells [70] at a multiplicity of infection of 2-5, then passaged on BHK-EnvA2

627   cells at a multiplicity of infection of 2. Purification, concentration, and titering were done as

628   described.

629   To make AAV1-CAG-Flpo virus, the Flpo gene [71] was cloned into pAAV-CAG-FLEX-

630   EGFP (Addgene 59331) to make pAAV-CAG-Flpo. Serotype 1 AAV was produced by triple

631   transfection of HEK 293T cells with pAAV-syn-Flpo, pAAV-RC1, and pHelper (Cellbiolabs

632   VPK-401) (per 15 cm plate, 15.5 ug, 21.0 ug, and 33.4 ug respectively) using Xfect (Clontech

633   631318) transfection reagent. Supernatants and cells were harvested at 72 hours posttransfection

634   and viruses purified and concentrated by iodixanol gradient centrifugation[72].

635   For quantification of dual-rabies retrograde tracing experiments from caudal and rostral

636   ACC, we sliced the brain into 100 µm sections and imaged GFP and/or tdTomato fluorescence

637   from every other slice using a 10x/0.4NA objective (Leica). Anatomical landmarks, such as

638   position/size of ventricles, corpus callosum, striatum, and hippocampus, were used to manually

639   align slices to a standard mouse brain atlas[46]. Back-labeled cells were counted using the cell

640   counter plugin in ImageJ (NIH). For the results presented in Figure 1C, we counted the number of

641   retrogradely neurons present in the different divisions of the visual cortex and normalized by the

642   total number of GFP- and tdTomato-expressing back-labeled cells found in the posterior cortex (0

643   to -4.0 mm posterior, relative to Bregma). For quantifying the distribution of cells projecting to

644   the intermediate and deep layers of the SC (Figure 1I), we counted the number of cells found in

645   the ACC as a function of distance from Bregma in 0.5mm bins. Since the sensory and

646 intermediate/motor layers of the superior colliculus are <0.5mm apart, it is challenging to restrict

647 virus injection to the motor layer. However, the frontal cortex predominantly projects only to the

648 motor layer; hence, to minimize contamination from virus spillover into the sensory layer of the

649 superior colliculus, we normalized the number of neurons in the ACC by the total number of back-

650 labeled neurons found in the frontal cortex (0 to +3mm anterior, relative to Bregma).

651   We injected rabies viruses encoding GFP or tdTomato into the visual cortex or the superior

652 colliculus to identify ACC neurons projecting to these structures. We counted the total number of

653 back-labeled neurons in the ACC (AP range 0 to 1mm) every 200 µm in each animal and quantified

654 the proportion of neurons that were labeled with GFP, tdTomato, or both out of all labeled cells.

655   We performed anterograde transsynaptic tracing experiments[56] to identify SC neurons that

656 receive inputs from the ACC using the AAV1-CAG-Flpo virus described above. We produced the

657 Flp-dependent tdTomato reporter line Ai65F by crossing the Cre- and Flp- dependent tdTomato

658 double-reporter line Ai65D [73] (Jackson Laboratory 021875) to the Cre deleter line Meox2-Cre [74]

659 (Jackson Laboratory 003755), so that only Flp is required for expression of tdTomato. An AAV1-

660 CAG-Flpo virus was injected in the ACC of these mice to label postsynaptic neurons with

661 tdTomato. After allowing 4-6 weeks for Flpo and tdTomato expression, we sectioned the brain

662 into 50µm slices and used standard immunohistochemistry techniques to identify GABA-

663 expressing neurons co-labeled with tdTomato. The tissue was placed in 5% normal goat serum,

664 1% triton blocking solution in 0.1M phosphate buffered saline (PBS) for 1 hour at room

665 temperature. It was then incubated in primary antibodies against GABA and NeuN (rabbit anti-

666 GABA, 1:500, A2052 Sigma; guinea pig anti-NeuN, 1:500, 266-004 Synaptic Systems) and 1%

667 NGS/ 0.5% triton overnight at 4ºC. Following washing in 0.1M PBS 3x10', the tissue was

668 incubated in secondary antibody (goat anti-rabbit IgG AlexaFluor 488, goat anti-guinea pig IgG

669 AlexaFluor 647, 1:500, Invitrogen) and 1% NGS for 4 hours at room temperature. Tissue was then

670 washed 3x10' in PBS, mounted, and coverslipped with anti-fade mounting medium (Prolong Gold,

671 ThermoFisher). Tiled z-stacks were collected on a confocal microscope (SP8, Leica) using a 20x

672 objective at 1024x1024 resolution, 2 µm apart (~20 z-slices) from sections containing the SC

673 (between -3.4 and -4.7 AP from bregma). A 1x1mm ROI was selected over the intermediate and

674 deep layers of SC and z-projected across 25µm. Background was automatically subtracted

675 (ImageJ), and NeuN+ cells were identified using an automated cell-counting binary mask

676 (watershed segmentation, ImageJ). GABA+/NeuN+ and tDTom+/GABA±/NeuN+ cells were

677 manually identified and calculated as the proportion of NeuN+ cells (cell-counter plugin, ImageJ).

678 Behavioral apparatus and task training: Mice were trained to report the spatial location of visual

679 cues by rotating a trackball left or right with their forepaws, similar to a previous design[10]. Animals

680 were headfixed on a behavior rig assembled from optical hardware (Thorlabs), placed in a

681 polypropylene tube to limit body movement, and positioned ~8 cm from an LCD screen (7"

682 diagonal; 700YV, Xenarc Direct) such that their forepaws rested on a trackball. Ball movements

683 were monitored with a commercially available USB optical trackball mouse (Kensington Expert

684 Mouse K64325). The original trackball was replaced with a 55mm diameter ping pong ball (Joola),

685 which was light enough for mice to rotate comfortably. We inserted a hypodermic tube down the

686 center of the trackball so it could only be rotated along a single axis (left or right). To fix the ping

687 pong ball to the optical mouse, we made grooves in the trackball chassis and secured the

688 hypodermic needle with hot glue. A USB host shield (SainSmart) was used to connect the output

689 of the optical mouse to a microcontroller (Arduino), which ran a custom routine that detected ball

690 movements every 10ms. In the event of a ball movement, the microcontroller outputted a

691 timestamp and the amount of movement (in pixels) to a behavioral control computer (Dell). In

692 addition, a time stamp was sent every 100ms to synchronize timing between the microcontroller

693 and the behavior computer. In our system, one pixel of optical mouse movement corresponded to

694 ~0.15° movement on the ball. Behavioral control was implemented with custom software written

695 in MATLAB (Mathworks) using the Psyhcophysics and the Data Acquisition toolboxes.

696 During the inward task (Figures 2-5), the presented visual cue (black square, ~20°) started

697 on either the left or the right side of the LCD screen. The trackball controlled the location of the

698 visual stimulus in closed loop in real-time. The gain of coupling between the trackball and the

699 stimulus was calibrated so that rotating the ball by the threshold amount (15°) in the correct

700 direction moved the stimulus from its starting position to the center of the screen. Ball positions

701 were accumulated throughout the trial until the stimulus reached the center or the response window

702 expired. Under this closed-loop control, any movement in the incorrect direction displaced the

703 stimulus farther away from the center and towards the edge of the screen. Hence, such movements

704 had to be offset by additional movements in the correct direction for the stimulus to move to the

705 center of the screen and for the trial to be considered correct. If the ball was moved opposite to the

39

706   direction of the instructed cue by the threshold amount, the stimulus moved to the edge of screen

707   and the trial was considered incorrect. The software operated similarly when mice were trained on

708   the outward contingency task (Figure 6), except that they were required to move the visual cue to

709   the edge of the screen for the trial to be considered correct, and moving the stimulus to the center

710   of the screen was considered an incorrect response. Water was given as reward on correct trials,

711   which was delivered through a metal spout placed within the reach of the tongue; the amount

712   dispensed was controlled by opening a solenoid valve for a calibrated period.

713   The following procedures were used to train mice on both the inward (Figure 2A) and

714   outward (Figure 6A) task contingencies. Mice were taken through successive stages of training

715   until they became proficient at the task. Once mice recovered from the surgery, they were water

716   restricted for 5-7 days ($\geq$ 1ml/day) and then trained to lick a metal spout to obtain small water

717   rewards (3-6 µL). If mice did not receive their water allotment during training, they were given

718   the remaining amount as hydrogel (Clear H_2O) in their home cage. After mice reliably licked the

719   waterspout, they earned water rewards by using the trackball to move the presented stimulus to the

720   center of the screen. To discourage spontaneous trackball movements, mice were required to hold

721   the ball still for 1s to trigger trial start, which was signaled with an auditory tone (0.5s, 1 KHz);

722   the visual cue appeared with a 1s delay after the onset of this tone. During early stages of training,

723   only movements in the correct direction contributed to movement of the stimulus. Once mice

724   reliably moved the ball in either direction on >90% of trials, this condition was removed, and the

725   movement of the stimulus was fully coupled to the movement of the trackball. In the next stage of

726   training, we used an anti-bias algorithm in which the same stimulus was repeated on consecutive

727   trials if mice made an error until they performed the trial correctly; stimulus location on trials

728   following correct trials were randomly chosen. Once performance reached ~70%, the anti-bias

729   algorithm was turned off and stimuli were presented in a randomized manner. Throughout all

730   stages, auditory white noise was used to signal miss trials if mice failed to move the ball to

731   threshold before expiration of the response window. As mice progressed through the training

732   stages, we gradually decreased the response window from 10s to 1s. Correct and incorrect trials

733   were signaled with auditory tones (0.2 kHz and 10kHz, respectively), followed by an inter-trial

734   delay of 2.5s.

735   Animals trained for two-photon imaging experiments were taken through two additional

736   stages of training. First, we turned off the closed loop coupling between the trackball and the

40

737　stimulus, and instead flashed stimuli for 200ms. This was to avoid the potential of evoking neural

738　activity due to the movement of the visual cue on the screen. Second, we introduced uncertainty

739　in temporal expectancy for stimulus onset by randomizing the period between the auditory cue

740　signaling trial start and the onset of the visual stimulus (exponential distribution with mean of ~1.8

741　seconds, min and max delay of 1 and 5s, respectively). Only mice trained for imaging experiments

742　were taken through these steps.

743　　　　A cohort of untrained mice were used to test the role of the SC in spontaneous trackball

744　movements. Mice received an injection of AAV-syn-Jaws in the SC and implanted with an optic

745　fiber cannula over the injection site, as described above. After mice recovered from surgery, they

746　were water restricted for 5-7 days and then trained to lick a metal spout to obtain small water

747　rewards (3-6 uL). Once mice reliably licked the waterspout, we began sessions of randomly

748　rewarded no-stimulus trials. During these sessions, no visual or auditory cues were presented that

749　would signal the beginning or end of each trial. No-stimulus "trials" of 2s duration were presented

750　continuously, such that there was no delay between the end of one trial and the beginning of the

751　next (note that this "trial" structure was not apparent to the mice, and is only used for administering

752　rewards, optogenetic stimulation, and subsequent analysis). On each trial, one movement direction,

753　clockwise or counterclockwise, was randomly selected by the software to be rewarded. If mice

754　moved the ball in the designated direction during this period, they obtained a small water reward;

755　no reward or feedback was provided for no-movement or "incorrect" trials (in which mice moved

756　the ball to threshold, but in the unrewarded direction). To encourage movements in both directions,

757　we simultaneously used two anti-bias algorithms during each session: 1) the movement direction

758　selected for rewarding was repeated on consecutive trials until mice received a reward; and 2) the

759　rewarded movement direction switched once mice received a reward.

760　Optogenetic manipulation of behavior: Photostimulation was provided with a solid state 593nm

761　laser for experiments using Jaws (OptoEngine). Laser stimulation was triggered from the behavior

762　control computer and lasted from 0.3s before to 1s after visual cue onset. ~20% of trials were

763　pseudorandomly selected for photostimulation. We additionally imposed the condition that

764　photostimulation could not occur on two consecutive trials. The output of the laser was coupled to

765　a patch cable (Thorlabs) with a FC/PC fiber coupler (OptoEngine). Laser power through the patch

766　cable was measured with a digital power meter before each experiment (Thorlabs). In experiments

767　requiring photostimulation through chronic windows over the visual cortex, the ceramic ferrule of

41

768   the patch cable was positioned so it filled the entire 3mm window and delivered a constant light

769   pulse with 20mW of power. In experiments requiring light delivery through implanted optical

770   fiber, the ceramic ferrule of the patch cable was coupled to the fiber optic cannula with a ferrule

771   mating sleeve (Thorlabs). Activity in the superior colliculus was inhibited by delivering 10mW of

772   constant yellow light. Photoinhibition of ACC outputs was achieved by constant yellow light

773   (20mW) illumination through an implanted fiber optic cannula (SC) or through a chronic window

774   (VC).

775   For optogenetic manipulation of spontaneous movements in untrained mice, an average of

776   39% (±15%) of "trials" were pseudorandomly selected for photostimulation, with the additional

777   stipulation that there be at least six consecutive trials (~12s) between laser trials. Laser stimulation

778   was triggered from the behavior control computer and lasted 1.3s, beginning from 0.3s before the

779   (uncued) trial start.

780   <u>Behavioral analysis for optogenetic experiments:</u> Trials were labeled as ipsi or contra depending

781   on the location of the presented visual cue relative to the brain hemisphere that was

782   photostimulated. We computed several metrics to quantify the performance on each trial type. The

783   timeout rate is the proportion of trials in which the ball was not moved to threshold within the

784   allotted response window out of all trials where a given stimulus was presented. The incorrect rate

785   is the proportion of trials in which the ball was moved opposite the direction instructed by the cue

786   out of all completed trials for each visual stimulus (i.e., excluding timeout trials). In other words,

787   100 – incorrect rate equals the correct rate. The response time was the amount of time taken from

788   stimulus onset to a complete correct response. The response window (i.e., time given for making

789   a complete response) was set to 1s.

790   Inactivation-induced change in counterclockwise (CCW) action bias shown in Figure 5D

791   and 6E was calculated as follows for the inward contingency task:

792
$$\Delta\,CCW\,response = \frac{(c_{corr,l} + i_{incorr,l}) - (c_{corr,nl} + i_{incorr,nl})}{(c_{corr,nl} + i_{incorr,nl})}$$

793   and for the outward contingency task:

794
$$\Delta\,CCW\,response = \frac{(i_{corr,l} + c_{incorr,l}) - (i_{corr,nl} + c_{incorr,nl})}{(i_{corr,nl} + c_{incorr,nl})}$$

795   The contra stimulus (CS) action bias in Figure 6D was computed as follows for both the inward

796   and outward tasks:

797
$$\Delta\ CS\ action\ bias = \frac{(c_{corr,l} + i_{incorr,l}) - (c_{corr,nl} + i_{incorr,nl})}{(c_{corr,nl} + i_{incorr,nl})}$$

798 In the equations above, c and i refer to contra and ipsi cues, *corr* and *incorr* refer to correct and

799 incorrect rates, and l and nl refer to laser and non-laser trials, respectively.

800 We quantified the effect of optogenetic inactivation on inward and outward tasks by

801 comparing behavioral performance on non-laser and laser trials from the same sessions. Data from

802 three optogenetic sessions were combined for each mouse. We used a permutation test to quantify

803 the significance of changes in behavioral performance observed with optogenetic inactivation. We

804 tested against the null hypothesis that the observed change in performance does not depend on

805 laser inactivation. In each round of permutation, we randomly reassigned the laser labels across

806 trials for each animal in an experiment. We then concatenated trials for all animals and recalculated

807 the average laser-induced change in the incorrect rate, the timeout rate, and the response time for

808 contra and ipsi cue trials. This process was repeated 1000 times, creating a distribution of

809 performance changes expected by chance. The two-tailed p-value was computed as the proportion

810 of performance changes that were as or more extreme than the observed change on either side of

811 the distribution. We determined significance using the Bonferroni adjusted alpha-value of 0.05/2

812 = 0.025 for analyses that compared the effect of inactivation on contra and ipsi cue trials.

813 We also tested the effect of optogenetic inactivation on spontaneous counterclockwise and

814 clockwise movements in untrained mice. Only trials with attempted movements, regardless of

815 whether they were rewarded, were considered for analysis. Trials in which the ball was moved by

816 the threshold amount of 5° were labeled as CW and CCW based on the direction of movement.

817 Inactivation induced changes in CW and CCW movements, shown in Supplementary Figure 3,

818 was calculated as follows:

819
$$\Delta\ CW\ Movement\ = \frac{(CW_l - CW_{nl})}{(CW_{nl})} \qquad \Delta\ CCW\ Movement\ = \frac{(CCW_l - CCW_{nl})}{(CCW_{nl})}$$

820 In the equations above, l and nl refer to laser and non-laser conditions, respectively; CW and CCW

821 refer to clockwise and counterclockwise direction of movements, respectively. We quantified the

822 effect of optogenetic inactivation by comparing attempted movements of each type in laser and

823 non-laser conditions. Though inactivation for this experiment was performed on either the left (n

824 = 2 mice) or right SC (n = 3 mice), movement directions were transposed in the analysis to make

825 all consistent with a left SC inactivation. That is, for mice with right SC inactivation, CW

43

826   movements were coded as CCW, and CCW movements were coded as CW; movement coding for

827   mice with left SC inactivation were left as is. Importantly, left and right SC inactivation had

828   opposite effects on movements; left SC inactivation decreased counterclockwise actions, whereas

829   right SC inactivation decreased clockwise actions. Trials from 4 sessions were concatenated for

830   each mouse. We used one-sample t-tests to test against the null hypothesis that observed changes

831   in CW or CCW movements for each mouse were significantly different from no change/zero. A

832   two-sample t-test was used to determine if changes in CW movements and CCW movements were

833   significantly different from each other.

834   <u>Two-photon microscopy:</u> GCaMP6s fluorescence was imaged through a 16x/0.8 NA objective

835   (Nikon) using galvo-galvo scanning with a Prairie Ultima IV two-photon microscopy system.

836   Excitation light at 910nm was provided by a tunable Ti:Sapphire laser (Mai-Tai eHP, Spectra-

837   Physics) equipped with dispersion compensation (DeepSee, Spectra-Physics). Emitted light was

838   collected with GaAsP photomultiplier tubes (PMTs; Hamamatsu). A blackout curtain attached to

839   a custom stainless-steel plate (eMachineShop.com), which was mounted on the headplate to

840   prevent light from the LCD screen from entering the PMTs. Layer 5 GCaMP6s-expressing neurons

841   in transgenic animals were imaged with 2x optical zoom, 350-550µm below the brain surface for

842   20-minute-long behavioral sessions. Upon completion, excitation wavelength was changed to

843   830nm, which produced both a signal from the retrobeads and a structural green signal from

844   GCaMP6. Emission signals were split with a dichroic mirror (FF649-Di01; Semrock) mounted in

845   a filter cube and directed to two different PMTs. Simultaneous imaging of both signals with 830nm

846   excitation facilitated spatial alignment of retrobead signals to GCaMP6s signals collected during

847   behavior and allowed us to identify SC-projecting ACC neurons (see 'Image analysis'). 4x optical

848   zoom was used for imaging callosal or visual cortex axons in the ACC up to 100µm below the

849   surface. All imaging experiments were performed at a frame rate of 5Hz. Laser power at the

850   specimen was controlled with pockel cells and ranged from 10 to 50 mW, depending on GCaMP6

851   expression levels and depth.

852   <u>Image analysis:</u> Images were acquired using the PrairieView software (Bruker) and saved as

853   multipage TIFF files using ImageJ (NIH). Image processing and region of interest (ROI) selection

854   was performed in ImageJ (NIH). To correct for lateralized movements in the x-y axis, images were

855   realigned to a reference frame (the pixel-wise mean of all frames) using the template matching

856　plugin [75]. ROIs were drawn manually over visually identified neurons using reference frames

857　generated by taking the pixel-wise maximum, mean, and standard deviation projection of all

858　frames. For each neuron, the same shaped ROI was also placed in an adjacent area devoid of other

859　neurons to estimate the background neuropil signal. To minimize the contribution of the neuropil

860　signal to the somatic signal, corrected neuronal fluorescence time series was estimated as $F(t) =$

861　$F_{raw\_soma}(t) - 0.7$ x $F_{raw\_neuropil}(t)$[76]. Similar image analysis was used for axonal imaging

862　experiments, except ROIs were drawn over visually-identified boutons and fluorescence signals

863　were not adjusted for neuropil contamination. $\Delta F/F$ (DFF) for each neuron or bouton was

864　calculated as $\Delta F/F(t) = 100$ x $(F(t) - F_0)/F_0$, where F_0 was the fluorescence value with the highest

865　density (estimated using MATLAB function ksdensity).

866　　　To identify retrobead-containing neurons, a reference frame was generated by taking the

867　pixel-wise mean of realigned GCaMP6s frames acquired during the behavioral session at 910nm.

868　The green channel acquired with excitation at 830nm was realigned to this reference using the

869　template matching plugin. The resulting translation values were then applied to the channel

870　containing signals from retrobeads. An average projection was taken after this realignment and

871　superimposed onto the 910 nm GCaMP reference frame used for drawing ROIs. Neurons

872　containing retrobeads were then visually identified.

873　<u>Analysis of visual activity in axons:</u> We assayed the visual responsiveness of visual cortex or

874　callosal axons in the ACC in animals passively viewing visual stimuli presented at the same

875　locations as during the task (solid black square for visual cortex axons, gratings drifting at 90º for

876　callosal axons; 1s stimulus duration). Visually responsive boutons were identified by comparing

877　pre-stimulus activity averaged over a 1s period to averaged activity 0.6s-1.2s after stimulus onset

878　(two-sided Wilcoxon signed-rank test, $P < 0.01$). AUROC values were computed for each bouton

879　using stimulus activity on contra and ipsi trials. A preference score was then computed as 2 x

880　(AUROC – 0.5); this score ranged from 1 (complete contra preference) to -1 (complete ipsi

881　preference). To determine if individual boutons had significant stimulus preference, scores were

882　recomputed after shuffling trial labels 1000 times. Observed preference scores outside the center

883　95% of the shuffled distribution were considered significant ($P < 0.05$, two-sided).

884　<u>Analysis of task responses of ACC neurons:</u> For imaging experiments during the inward

885　contingency task (Figures 2, 3), the session-wide DFF trace for each neuron was z-score

45

886   normalized. Responses on individual trials were aligned to visual stimulus onset. Trials were
887   labeled as contra-counterclockwise, contra-clockwise, ipsi-counterclockwise, and ipsi-clockwise
888   depending on the location of the visual cue relative to the hemisphere imaged and the action
889   selected by the animal. We only analyzed sessions with at least 5 trials in each condition (note that
890   the contra-clockwise and ipsi-counterclockwise conditions correspond to incorrect trials). The
891   color plots in Figure 2F and 3D were generated by averaging responses on each trial condition for
892   each neuron. Note that rows correspond to neurons, and each row plots activity of the same neurons
893   across the four conditions. For analyses in Figures 2G, H and 3E, responses were averaged over a
894   1s post-stimulus period (post-stimulus response) and then compared for the indicated trial
895   conditions using Wilcoxon signed-rank tests. To determine trial activity on contra cue trials
896   (Figure 2H), we first separately averaged post-stimulus responses on contra-counterclockwise and
897   contra-clockwise trials; responses on these trial types were then averaged together to generate
898   contra responses. Trial activity on ipsi cue, counterclockwise, and clockwise trials was determined
899   similarly, except post-stimulus responses on the following trial types were used, respectively: 1)
900   ipsi-counterclockwise and ipsi-clockwise; 2) contra-counterclockwise and ipsi-counterclockwise;
901   and 3) contra-clockwise and ipsi-clockwise.

902   Decoding actions from neuronal activity: We built linear support vector machine (SVM)
903   classifiers using the LIBSVM library for MATLAB[77] to test whether the activity of ACC-SC
904   neurons can be used to predict which action was selected by the animal. Selection of the
905   regularization parameter C was performed with a dataset not included in the analysis (unlabled
906   ACC neurons). We tested a range of values for C and selected the one which gave the best classifier
907   accuracy on a 10-fold cross-validated dataset. For this procedure, the classifier was trained to
908   distinguish between contra-CCW and ipsi-CW trials.

909   Since we simultaneously recorded only a few ACC-SC neurons, we constructed
910   'pseudotrials' by combining neuronal responses recorded across different sessions. SVM classifier
911   was trained to predict CCW or CW trials based on post-stimulus activity (z-scored DFF averaged
912   over 1s after stimulus onset) on individual trials. Activity for the CCW label was taken from
913   contra-CCW and ipsi-CCW, and for the CW label from contra-CW and ipsi-CW trials (also see
914   schematic in Figure 3F). We ran 1000 iterations of the model. There was an unequal number of
915   trials between conditions, so we used subsampling to balance trial types on each iteration (5 trials
916   from each condition). We minimized model over-fitting by using the cross-validation technique

46

917 (10-fold) to split the data into a training and testing set on each iteration. Classifier performance

918 on each iteration was estimated by averaging prediction accuracies across the 10 splits. Final

919 classifier accuracy was determined by averaging these mean accuracies across all iterations. To

920 determine if the action decoder performed above chance, we used an identical procedure except

921 we shuffled labels for the test data. Mean prediction accuracy derived from correctly labeled test

922 data and falling outside the center 95% of the shuffled distribution was considered significant.

923 Electrophysiological recordings in the SC: For photostimulation of the ACC, we injected

924 AAV1.CaMKII.hChR2(H134R)-mCherry (University of Pennsylvania vector core) at coordinates

925 AP: 0.5mm, ML: 0.5mm, and DV: 0.4 and 0.9mm (250 nL at each site). Cannulas were implanted

926 such that the optical fiber was 0.3mm below the pia (300µm/0.39NA core fiber optic coupled to a

927 2.5mm stainless steel ferrule; CFMC13L02, Thorlabs). We tested the effect of photostimulating

928 ChR2-expressing ACC neurons on activity in the SC using a 473nm blue solid state laser

929 (Optoengine). One or two days before the experiments, mice were habituated to head-fixation in

930 1h sessions. On the day of the experiment, mice were anesthetized with isoflurane and the

931 Metabond and silicone elastomer on the skull were removed. The mouse was placed on the

932 stereotaxic frame and a 500 µm diameter craniotomy was performed on top of the recording site

933 (from bregma: -3.6 to -4 mm anteroposterior and 0.8 to 1 mm mediolateral). The dura above the

934 cortex was removed and the craniotomy was protected with saline and a piece of gelfoam. SC

935 craniotomy was performed on the same side as that implanted with the fiber optic cannula over the

936 ACC. The skull was covered again with silicone elastomer and the animal was returned to its home

937 cage to recover from anesthesia for at least 2 hours. After recovery, mice were headfixed and the

938 silicone and gelfoam overlaying the craniotomy was gently removed. 0.9% NaCl solution was used

939 to keep the surface of the brain wet for the duration of the recordings.

940 After placing the animal in the recording set up, we submerged a reference silver wire in

941 the NaCl solution on the skull surface. The position of the 16-channel silicone probe (A1x16-

942 Poly2-5mm-50s-177-A16, NeuroNexus) was referenced on lambda and the surface of the brain

943 and lowered slowly (1 min per mm) to reach superficial sensory layer of the superior colliculus

944 (~1.3 mm in the ventral axis) using a motorized micromanipulator (MP – 285; Sutter Instrument

945 Company). The extracellular signal was amplified using a 1x gain headstage (model E2a; Plexon)

946 connected to a 50x preamp (PBX-247; Plexon) and digitalized at 50 kHz. The signal was highpass

947 filtered at 300Hz. Once the visual layer of the SC was identified (characterized by strong and

47

948   reliable visual responses to drifting gratings and sparse noise), the recording probe was lowered

949   ~400 μm deeper to the motor layer of the SC. For successful recordings, the silicone probe was

950   gently retracted and the recording tract was marked by re-entering the DiI coated probe (2 mg/mL

951   – D3911, ThermoFisher Scientific) at the same location. For some experiments, we were able to

952   record from two locations spaced 500μm apart in the dorsal-ventral axis. The brain was harvested

953   post-hoc and sectioned to confirm the probe location and ChR2 expression in the ACC. Spikes

954   were isolated online with amplitude threshold using Plexon Recorder software, but re-sorted using

955   the MountainSort automated spike sorting algorithm[78]. Units were curated manually after

956   automatic detection.

957   Visual stimuli were presented during recordings in the SC to increase neuronal

958   responsiveness. Sparse noise on a 3 x 5 grid (square size was the same as used for behavior

959   experiments) of black and white square on a gray background (50% luminance) were displayed

960   for 0.1s, followed by a 0.1s gray screen period. Positions were randomized within each block such

961   that black and white squares were presented once at each of the 15 positions. The total duration of

962   a block was 6 sec, with 1s inter-block intervals. Photostimulation of the ACC (10ms blue light

963   pulses at 20 Hz) was performed on 50% of the blocks. Photostimulation started 0.5s before visual

964   stimulus presentation and was turned off 0.5s after stimulus offset (total duration of 7s).

965   Since ACC axons in the SC target the intermediate and deep layers, we focused our analysis

966   on recordings made from these areas. While we observed robust retinotopically organized visual

967   responses in the superficial layer, we rarely encountered cells in the deeper layers that specifically

968   responded to the location of sparse noise stimuli. Therefore, recordings from deeper neurons likely

969   reflect ongoing, spontaneous activity that is modulated by the visual stimulation. We first

970   determined if individual neurons were significantly modulated by laser activation of the ACC by

971   comparing the firing rates (FR) of activity on non-laser and laser trials. For each modulated neuron,

972   we also computed a laser modulation index using the following equation:

973
$$\frac{FR_{Laser} - FR_{nonlaser}}{FR_{Laser} + FR_{nonlaser}}$$

974

References

1   Pinto, L. & Dan, Y. Cell-type-specific activity in prefrontal cortex during goal-directed behavior. *Neuron* **87**, 437-450, doi:10.1016/j.neuron.2015.06.021 (2015).

2   Goard, M. J., Pho, G. N., Woodson, J. & Sur, M. Distinct roles of visual, parietal, and frontal motor cortices in memory-guided sensorimotor decisions. *Elife* **5**, doi:10.7554/eLife.13764 (2016).

3   Li, N., Chen, T. W., Guo, Z. V., Gerfen, C. R. & Svoboda, K. A motor cortex circuit for motor planning and movement. *Nature* **519**, 51-56, doi:10.1038/nature14178 (2015).

4   Britten, K. H., Shadlen, M. N., Newsome, W. T. & Movshon, J. A. The analysis of visual motion: a comparison of neuronal and psychophysical performance. *J Neurosci* **12**, 4745-4765 (1992).

5   Erlich, J. C., Bialek, M. & Brody, C. D. A cortical substrate for memory-guided orienting in the rat. *Neuron* **72**, 330-343, doi:10.1016/j.neuron.2011.07.010 (2011).

6   Burgess, C. P. *et al.* High-Yield Methods for Accurate Two-Alternative Visual Psychophysics in Head-Fixed Mice. *Cell Rep* **20**, 2513-2524, doi:10.1016/j.celrep.2017.08.047 (2017).

7   Raposo, D., Kaufman, M. T. & Churchland, A. K. A category-free neural population supports evolving demands during decision-making. *Nat Neurosci* **17**, 1784-1792, doi:10.1038/nn.3865 (2014).

8   Harvey, C. D., Coen, P. & Tank, D. W. Choice-specific sequences in parietal cortex during a virtual-navigation decision task. *Nature* **484**, 62-68, doi:10.1038/nature10918 (2012).

9   Felsen, G. & Mainen, Z. F. Neural Substrates of Sensory-Guided Locomotor Decisions in the Rat Superior Colliculus. *Neuron* **60**, 137-148, doi:https://doi.org/10.1016/j.neuron.2008.09.019 (2008).

10   Sanders, J. I. & Kepecs, A. Choice ball: a response interface for two-choice psychometric discrimination in head-fixed mice. *J Neurophysiol* **108**, 3416-3423, doi:10.1152/jn.00669.2012 (2012).

11   Miller, E. K. & Cohen, J. D. An integrative theory of prefrontal cortex function. *Annu Rev Neurosci* **24**, 167-202, doi:10.1146/annurev.neuro.24.1.167 (2001).

12   Wimmer, R. D. *et al.* Thalamic control of sensory selection in divided attention. *Nature* **526**, 705, doi:10.1038/nature15398 (2015).

13   Cohen, J. D., McClure, S. M. & Angela, J. Y. Should I stay or should I go? How the human brain manages the trade-off between exploitation and exploration. *Philosophical Transactions of the Royal Society of London B: Biological Sciences* **362**, 933-942 (2007).

14   Moore, T. & Fallah, M. Control of eye movements and spatial attention. *Proceedings of the National Academy of Sciences* **98**, 1273-1276, doi:10.1073/pnas.021549498 (2001).

15   Grunfeld, I. S. & Likhtik, E. Mixed selectivity encoding and action selection in the prefrontal cortex during threat assessment. *Current opinion in neurobiology* **49**, 108-115, doi:10.1016/j.conb.2018.01.008 (2018).

16   Gregoriou, G. G., Gotts, S. J. & Desimone, R. Cell-type-specific synchronization of neural activity in FEF with V4 during attention. *Neuron* **73**, 581-594, doi:10.1016/j.neuron.2011.12.019 (2012).

17   Zhang, S. *et al.* Selective attention. Long-range and local circuits for top-down modulation of visual cortex processing. *Science* **345**, 660-665, doi:10.1126/science.1254126 (2014).

18   White, M. G. *et al.* Anterior Cingulate Cortex Input to the Claustrum Is Required for Top-Down Action Control. *Cell Reports* **22**, 84-95, doi:https://doi.org/10.1016/j.celrep.2017.12.023 (2018).

19   Moore, T. & Armstrong, K. M. Selective gating of visual signals by microstimulation of frontal cortex. *Nature* **421**, 370-373, doi:10.1038/nature01341 (2003).

20   Moore, T. & Fallah, M. Microstimulation of the frontal eye field and its effects on covert spatial attention. *J Neurophysiol* **91**, 152-162, doi:10.1152/jn.00741.2002 (2004).

21   Tehovnik, E. J., Sommer, M. A., Chou, I. H., Slocum, W. M. & Schiller, P. H. Eye fields in the frontal lobes of primates. *Brain Res Brain Res Rev* **32**, 413-448, doi:10.1016/s0165-0173(99)00092-2 (2000).

22   Schafer, R. J. & Moore, T. Selective attention from voluntary control of neurons in prefrontal cortex. *Science* **332**, 1568-1571, doi:10.1126/science.1199892 (2011).

23   Fillinger, C., Yalcin, I., Barrot, M. & Veinante, P. Afferents to anterior cingulate areas 24a and 24b and midcingulate areas 24a' and 24b' in the mouse. *Brain Struct Funct* **222**, 1509-1532, doi:10.1007/s00429-016-1290-1 (2017).

24   Huda, R., Pho, G. N., Wickersham, I. R. & Sur, M. in *Society for Neuroscience.*

25   Murakami, T., Yoshida, T., Matsui, T. & Ohki, K. Wide-field Ca(2+) imaging reveals visually evoked activity in the retrosplenial area. *Front Mol Neurosci* **8**, 20, doi:10.3389/fnmol.2015.00020 (2015).

26   Koike, H. *et al.* Chemogenetic Inactivation of Dorsal Anterior Cingulate Cortex Neurons Disrupts Attentional Behavior in Mouse. *Neuropsychopharmacology* **41**, 1014-1023, doi:10.1038/npp.2015.229 (2016).

27   Zhang, S. *et al.* Long-range and local circuits for top-down modulation of visual cortex processing. *Science* **345**, 660-665, doi:10.1126/science.1254126 (2014).

28   Leinweber, M., Ward, D. R., Sobczak, J. M., Attinger, A. & Keller, G. B. A Sensorimotor Circuit in Mouse Cortex for Visual Flow Predictions. *Neuron* **95**, 1420-1432.e1425, doi:https://doi.org/10.1016/j.neuron.2017.08.036 (2017).

29   Zhang, S. *et al.* Organization of long-range inputs and outputs of frontal cortex for top-down control. *Nature Neuroscience* **19**, 1733, doi:10.1038/nn.4417 (2016).

30   Hu, F. *et al.* Prefrontal Corticotectal Neurons Enhance Visual Processing through the Superior Colliculus and Pulvinar Thalamus. *Neuron* (2019).

31   Fillinger, C., Yalcin, I., Barrot, M. & Veinante, P. Efferents of anterior cingulate areas 24a and 24b and midcingulate areas 24a' and 24b' in the mouse. *Brain Struct Funct* **223**, 1747-1778, doi:10.1007/s00429-017-1585-x (2018).

32   Schiller, P. H., Sandell, J. H. & Maunsell, J. H. The effect of frontal eye field and superior colliculus lesions on saccadic latencies in the rhesus monkey. *J Neurophysiol* **57**, 1033-1049, doi:10.1152/jn.1987.57.4.1033 (1987).

33   Krauzlis, R. J., Lovejoy, L. P. & Zenon, A. Superior colliculus and visual spatial attention. *Annu Rev Neurosci* **36**, 165-182, doi:10.1146/annurev-neuro-062012-170249 (2013).

34   Wolf, A. B. *et al.* An integrative role for the superior colliculus in selecting targets for movements. *J Neurophysiol* **114**, 2118-2131, doi:10.1152/jn.00262.2015 (2015).

35   Robinson, D. A. Eye movements evoked by collicular stimulation in the alert monkey. *Vision Res* **12**, 1795-1808 (1972).

36   Dean, P., Mitchell, I. J. & Redgrave, P. Contralateral head movements produced by microinjection of glutamate into superior colliculus of rats: evidence for mediation by multiple output pathways. *Neuroscience* **24**, 491-500 (1988).

37   Knudsen, E. I. Neural Circuits That Mediate Selective Attention: A Comparative Perspective. *Trends Neurosci* **41**, 789-805, doi:10.1016/j.tins.2018.06.006 (2018).

38   Glimcher, P. W. & Sparks, D. L. Movement selection in advance of action in the superior colliculus. *Nature* **355**, 542-545, doi:10.1038/355542a0 (1992).

39   Liang, F. *et al.* Sensory Cortical Control of a Visually Induced Arrest Behavior via Corticotectal Projections. *Neuron* **86**, 755-767, doi:10.1016/j.neuron.2015.03.048 (2015).

40   Crapse, T. B., Lau, H. & Basso, M. A. A Role for the Superior Colliculus in Decision Criteria. *Neuron* **97**, 181-194 e186, doi:10.1016/j.neuron.2017.12.006 (2018).

41   Hirokawa, J. *et al.* Multisensory information facilitates reaction speed by enlarging activity difference between superior colliculus hemispheres in rats. *PLoS One* **6**, e25283, doi:10.1371/journal.pone.0025283 (2011).

42   Stubblefield, E. A., Costabile, J. D. & Felsen, G. Optogenetic investigation of the role of the superior colliculus in orienting movements. *Behav Brain Res* **255**, 55-63, doi:10.1016/j.bbr.2013.04.040 (2013).

43   Duan, C. A., Erlich, J. C. & Brody, C. D. Requirement of Prefrontal and Midbrain Regions for Rapid Executive Control of Behavior in the Rat. *Neuron* **86**, 1491-1503, doi:10.1016/j.neuron.2015.05.042 (2015).

44   Gandhi, N. J. & Katnani, H. A. Motor functions of the superior colliculus. *Annu Rev Neurosci* **34**, 205-231, doi:10.1146/annurev-neuro-061010-113728 (2011).

45   Zenon, A. & Krauzlis, R. J. Attention deficits without cortical neuronal deficits. *Nature* **489**, 434-437, doi:10.1038/nature11497 (2012).

46   Paxinos, G. & Franklin, K. B. *Paxinos and Franklin's the mouse brain in stereotaxic coordinates*. (Academic press, 2019).

47   Kvitsiani, D. *et al.* Distinct behavioural and network correlates of two interneuron types in prefrontal cortex. *Nature* **498**, 363-366, doi:10.1038/nature12176 (2013).

48   Allsop, S. A. *et al.* Corticoamygdala Transfer of Socially Derived Information Gates Observational Learning. *Cell* **173**, 1329-1342 e1318, doi:10.1016/j.cell.2018.04.004 (2018).

49   Weible, A. P., Rowland, D. C., Monaghan, C. K., Wolfgang, N. T. & Kentros, C. G. Neural correlates of long-term object memory in the mouse anterior cingulate cortex. *J Neurosci* **32**, 5598-5608, doi:10.1523/JNEUROSCI.5265-11.2012 (2012).

50   Wang, Q. & Burkhalter, A. Area map of mouse visual cortex. *Journal of Comparative Neurology* **502**, 339-357, doi:doi:10.1002/cne.21286 (2007).

51   Svoboda, K. & Li, N. Neural mechanisms of movement planning: motor cortex and beyond. *Curr Opin Neurobiol* **49**, 33-41, doi:10.1016/j.conb.2017.10.023 (2018).

52   Chuong, A. S. *et al.* Noninvasive optical inhibition with a red-shifted microbial rhodopsin. *Nat Neurosci* **17**, 1123-1129, doi:10.1038/nn.3752 (2014).

53   Steinmetz, N. A., Zatka-Haas, P., Carandini, M. & Harris, K. D. Distributed coding of choice, action and engagement across the mouse brain. *Nature*, doi:10.1038/s41586-019-1787-x (2019).

54   Hikosaka, O., Takikawa, Y. & Kawagoe, R. Role of the basal ganglia in the control of purposive saccadic eye movements. *Physiol Rev* **80**, 953-978, doi:10.1152/physrev.2000.80.3.953 (2000).

55   Doykos, T. K., Gilmer, J. I., Person, A. L. & Felsen, G. Monosynaptic Inputs to Excitatory and Inhibitory Neurons of the Intermediate and Deep Layers of the Superior Colliculus. *bioRxiv*, 824250 (2019).

56   Zingg, B. *et al.* AAV-Mediated Anterograde Transsynaptic Tagging: Mapping Corticocollicular Input-Defined Neural Pathways for Defense Behaviors. *Neuron* **93**, 33-47, doi:https://doi.org/10.1016/j.neuron.2016.11.045 (2017).

57   Glickfeld, L. L., Histed, M. H. & Maunsell, J. H. Mouse primary visual cortex is used to detect both orientation and contrast changes. *J Neurosci* **33**, 19416-19422, doi:10.1523/JNEUROSCI.3560-13.2013 (2013).

58   Munoz, D. P. & Istvan, P. J. Lateral inhibitory interactions in the intermediate layers of the monkey superior colliculus. *J Neurophysiol* **79**, 1193-1209, doi:10.1152/jn.1998.79.3.1193 (1998).

59   Felsen, G. & Mainen, Z. F. Midbrain contributions to sensorimotor decision making. *J Neurophysiol* **108**, 135-147, doi:10.1152/jn.01181.2011 (2012).

60   Lo, C. C. & Wang, X. J. Cortico-basal ganglia circuit mechanism for a decision threshold in reaction time tasks. *Nat Neurosci* **9**, 956-963, doi:10.1038/nn1722 (2006).

61   Takahashi, M., Sugiuchi, Y. & Shinoda, Y. Topographic organization of excitatory and inhibitory commissural connections in the superior colliculi and their functional roles in saccade generation. *J Neurophysiol* **104**, 3146-3167, doi:10.1152/jn.00554.2010 (2010).

62   Takahashi, M. Morphological and electrophysiological characteristics of the commissural system in the superior colliculi for control of eye movements. *Prog Brain Res* **249**, 105-115, doi:10.1016/bs.pbr.2019.04.027 (2019).

63   Munoz, D. P. & Everling, S. Look away: the anti-saccade task and the voluntary control of eye movement. *Nat Rev Neurosci* **5**, 218-228, doi:10.1038/nrn1345 (2004).

64   Kojima, S. & Goldman-Rakic, P. S. Delay-related activity of prefrontal neurons in rhesus monkeys performing delayed response. *Brain Res* **248**, 43-49, doi:10.1016/0006-8993(82)91145-3 (1982).

65   Guo, Z. V. *et al.* Flow of cortical activity underlying a tactile decision in mice. *Neuron* **81**, 179-194, doi:10.1016/j.neuron.2013.10.020 (2014).

66   Wang, M. *et al.* Macaque dorsal premotor cortex exhibits decision-related activity only when specific stimulus-response associations are known. *Nat Commun* **10**, 1793, doi:10.1038/s41467-019-09460-y (2019).

67   Zhao, X., Liu, M. & Cang, J. Visual cortex modulates the magnitude but not the selectivity of looming-evoked responses in the superior colliculus of awake mice. *Neuron* **84**, 202-213, doi:10.1016/j.neuron.2014.08.037 (2014).

68   Wallace, S. F., Rosenquist, A. C. & Sprague, J. M. Ibotenic acid lesions of the lateral substantia nigra restore visual orientation behavior in the hemianopic cat. *J Comp Neurol* **296**, 222-252, doi:10.1002/cne.902960204 (1990).

69   Wickersham, I. R. & Sullivan, H. A. Rabies viral vectors for monosynaptic tracing and targeted transgene expression in neurons. *Cold Spring Harb Protoc* **2015**, 375-385, doi:10.1101/pdb.prot072389 (2015).

70   Wickersham, I. R., Sullivan, H. A. & Seung, H. S. Production of glycoprotein-deleted rabies viruses for monosynaptic tracing and high-level gene expression in neurons. *Nat Protoc* **5**, 595-606, doi:10.1038/nprot.2009.248 (2010).

71   Raymond, C. S. & Soriano, P. High-efficiency FLP and PhiC31 site-specific recombination in mammalian cells. *PLoS One* **2**, e162, doi:10.1371/journal.pone.0000162 (2007).

72   Choi, V. W., Asokan, A., Haberman, R. A., McCown, T. J. & Samulski, R. J. Production of recombinant adeno-associated viral vectors and use for in vitro and in vivo

1156 administration. *Curr Protoc Neurosci* **Chapter 4**, Unit 4 17,
1157 doi:10.1002/0471142301.ns0417s35 (2006).
1158 73 Madisen, L. *et al.* Transgenic mice for intersectional targeting of neural sensors and
1159 effectors with high specificity and performance. *Neuron* **85**, 942-958,
1160 doi:10.1016/j.neuron.2015.02.022 (2015).
1161 74 Tallquist, M. D. & Soriano, P. Epiblast-restricted Cre expression in MORE mice: a tool to
1162 distinguish embryonic vs. extra-embryonic gene function. *Genesis* **26**, 113-115 (2000).
1163 75 Tseng, Q. *et al.* A new micropatterning method of soft substrates reveals that different
1164 tumorigenic signals can promote or reduce cell contraction levels. *Lab on a chip* **11**, 2231-
1165 2240 (2011).
1166 76 Chen, T.-W. *et al.* Ultrasensitive fluorescent proteins for imaging neuronal activity. *Nature*
1167 **499**, 295, doi:10.1038/nature12354 (2013).
1168 77 Chang, C.-C. & Lin, C.-J. LIBSVM: A library for support vector machines. *ACM*
1169 *transactions on intelligent systems and technology (TIST)* **2**, 27 (2011).
1170 78 Chung, J. E. *et al.* A Fully Automated Approach to Spike Sorting. *Neuron* **95**, 1381-1394
1171 e1386, doi:10.1016/j.neuron.2017.08.030 (2017).